



Emissions and atmospheric processes influence the chemical composition and toxicological properties of urban air particulate matter in Nanjing, China



Teemu J. Rönkkö ^{a,*}, Pasi I. Jalava ^a, Mikko S. Happo ^a, Stefanie Kasurinen ^a, Olli Sippula ^a, Ari Leskinen ^{b,c}, Hanna Koponen ^a, Kari Kuuspalo ^a, Jarno Ruusunen ^a, Olli Väisänen ^c, Liqing Hao ^c, Antti Ruuskanen ^b, Jürgen Orasche ^{d,e}, Die Fang ^f, Lei Zhang ^f, Kari E.J. Lehtinen ^{b,c}, Yu Zhao ^f, Cheng Gu ^f, Qin'geng Wang ^f, Jorma Jokiniemi ^a, Mika Komppula ^b, Maija-Riitta Hirvonen ^a

^a University of Eastern Finland, Department of Environmental and Biological Sciences, Yliopistonranta 1, P.O. Box 1627, FI-70211 Kuopio, Finland

^b Finnish Meteorological Institute, Yliopistonranta 1, P.O. Box 1627, FI-70211 Kuopio, Finland

^c University of Eastern Finland, Department of Applied Physics, Yliopistonranta 1, P.O. Box 1627, FI-70211 Kuopio, Finland

^d German Research Center for Environmental Health, Helmholtz Zentrum München, Munich, Germany

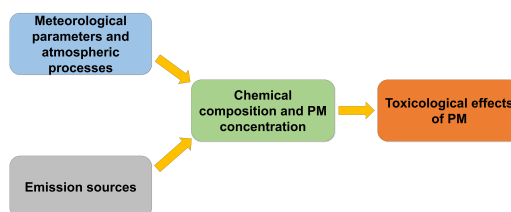
^e Joint Mass Spectrometry Center, Cooperation Group Comprehensive Molecular Analytics, German Research Center for Environmental Health, Helmholtz Zentrum München, Munich, Germany

^f Nanjing University, School of the Environment, Branch 24 Mailbox of Nanjing University Xianlin Campus, No. 163 Xianlin Avenue, Qixia District, 210023 Nanjing, China

HIGHLIGHTS

- Emission sources and atmospheric processes dictate the chemical composition of PM.
- The chemical composition of PM showed seasonal and day-night variations.
- Differences in chemical composition affect the toxicological responses.
- PM size fractions cause toxicity via different pathways.

GRAPHICAL ABSTRACT



ARTICLE INFO

Article history:

Received 14 February 2018

Received in revised form 21 May 2018

Accepted 22 May 2018

Available online 26 May 2018

Editor: Jianmin Chen

Keywords:

Air pollution

Cytotoxicity

Genotoxicity

Inflammation

In vitro toxicology

ABSTRACT

Ambient inhalable particulate matter (PM) is a serious health concern worldwide, but especially so in China where high PM concentrations affect huge populations. Atmospheric processes and emission sources cause spatial and temporal variations in PM concentration and chemical composition, but their influence on the toxicological characteristics of PM are still inadequately understood.

In this study, we report an extensive chemical and toxicological characterization of size-segregated urban air inhalable PM collected in August and October 2013 from Nanjing, and assess the effects of atmospheric processes and likely emission sources. A549 human alveolar epithelial cells were exposed to day- and nighttime PM samples (25, 75, 150, 200, 300 µg/ml) followed by analyses of cytotoxicity, genotoxicity, cell cycle, and inflammatory response.

PM_{10–2.5} and PM_{0.2} caused the greatest toxicological responses for different endpoints, illustrating that particles with differing size and chemical composition activate distinct toxicological pathways in A549 cells. PM_{10–2.5} displayed the greatest oxidative stress and genotoxic responses; both were higher for the August samples compared with October. In contrast, PM_{0.2} and PM_{2.5–1.0} samples displayed high cytotoxicity and substantially disrupted cell cycle; August samples were more cytotoxic whereas October samples displayed higher cell cycle disruption. Several components associated with combustion, traffic, and industrial emissions displayed strong correlations with these toxicological responses. The lower responses for PM_{1.0–0.2} compared to PM_{0.2} and

* Corresponding author.

E-mail address: teemu.ronkko@uef.fi (T.J. Rönkkö).

$\text{PM}_{2.5-1.0}$ indicate diminished toxicological effects likely due to aerosol aging and lower proportion of fresh emission particles rich in highly reactive chemical components in the $\text{PM}_{1.0-0.2}$ fraction. Different emission sources and atmospheric processes caused variations in the chemical composition and toxicological responses between PM fractions, sampling campaigns, and day and night. The results indicate different toxicological pathways for coarse-mode particles compared to the smaller particle fractions with typically higher content of combustion-derived components. The variable responses inside PM fractions demonstrate that differences in chemical composition influence the induced toxicological responses.

© 2018 The Authors. Published by Elsevier B.V. This is an open access article under the CC BY license (<http://creativecommons.org/licenses/by/4.0/>).

1. Introduction

China's rapid economic growth has led to severely elevated levels of particulate matter (PM) air pollution, which has been witnessed during recent years in phenomena such as haze and smog. Most harshly affected by PM pollution are the economically developed, heavily industrialized and densely populated urban areas, such as the provincial capitals (Chen and Xu, 2017). One of these capital cities is Nanjing, located in the Yangtze River Delta (YRD) region in southeastern China; it is a major industrial, commercial and educational hub of the Jiangsu province, which has recently experienced severe air pollution events. Chronic exposure to ambient air pollution is associated with increased mortality and morbidity, including increased risk of cardiopulmonary diseases such as chronic obstructive pulmonary disease (COPD), and is considered one of the greatest global risk factors for human health (Cohen et al., 2017; Forouzanfar et al., 2015; Lim et al., 2012). Recent evidence shows that ambient air pollution can also increase the risk of a diverse set of diseases, such as diabetes and Alzheimer's (Maher et al., 2016; Mazidi and Speakman, 2017; Pearson et al., 2010). Exposure to $\text{PM}_{2.5}$, particulate matter with aerodynamic diameter under $2.5 \mu\text{m}$, was the fifth-ranking mortality risk factor globally in 2015, with an estimated 4.2 million attributable premature deaths (7.6% of total global mortality), whereof 1.1 million occurred in China (Cohen et al., 2017). In East Asia, PM_{2.5} emissions by the residential and commercial sector were estimated to contribute to 21% of total anthropomorphic PM_{2.5} mortality, followed by industrial (17%) and energy (11%) sectors (Silva et al., 2016). The combination of high air pollution levels and high population density makes air pollution a particularly serious threat to public health in East Asia; thus, it has prompted new policies to counter the problem by the Chinese government.

The current laws and regulations concerning PM emissions are based on particle mass concentrations of selected size-fractions (PM₁₀ and PM_{2.5}), considering all particles equally toxic and discarding the effect of chemical composition of particles to induced adverse health effects (United States Clean Air Act, European Union Directive 2008/50/EC). Many studies have demonstrated that the most prominent representatives for the induced toxic responses have been heavy metals, and organic and elemental carbon content, which increase inflammation, cytotoxicity and tissue damage. Indeed, several polycyclic aromatic hydrocarbons (PAHs) occurring in PM have been shown to have high genotoxic and carcinogenic activities, but also modulate immunological responses (Ghio et al., 2014; Happo et al., 2007; Hoppo et al., 2008; Hoppo et al., 2010b; Hetland et al., 2001; Jalava et al., 2015; Schwarze et al., 2006). The composition of the particles is profoundly influenced by the local emission sources and prevailing atmospheric and meteorological conditions, showing significant spatial and temporal variations (Hoppo et al., 2010a; Jalava et al., 2007; Jalava et al., 2009). The different conditions and emission sources during day and night cause another level of variation (Jalava et al., 2015). Despite the evidence of composition-based variations in PM-induced adverse effects, no clear causal relationships between certain components and morbidity and mortality have been reported. Because of the large effect of emission sources on PM toxicity, it is very important to specify the role of emission sources, conditions, as well as natural characteristics, especially in areas of enormously high PM concentrations with high population densities.

To depict an overall picture of harmful emission sources, air quality and the toxicity of local PM mixture in Nanjing, we performed two distinct sampling campaigns followed by the subsequent extensive chemical and toxicological characterization of the samples. Thus, the specific aims of our present study were two-fold. Firstly, we assessed the seasonal and day-night variations of the measured atmospheric processes and meteorological parameters, and how large an effect they had on the size-segregated PM concentrations and on the chemical composition of particles. Secondly, we assessed how this variation influenced PM toxicity using the human alveolar epithelial cell line A549. To reach this goal, we determined the PM-induced changes of cellular metabolic activity, cell membrane integrity, oxidative stress, DNA damage, cell cycle phase and inflammatory response. These toxicological data were combined with the chemical characterization of the studied PM and online meteorological data to provide an extensive analysis of how atmospheric processes and chemical composition influence the toxicological characteristics of PM. The sampling campaigns were chosen to represent two distinct air quality conditions, hot August representing fast atmospheric chemical aging of PM components, whereas in October, after the harvest, regional burning of agricultural residue crop becomes a major source of PM and can lead to severe air pollution events (Chen et al., 2017a; Zhao et al., 2015; Zhu et al., 2010).

2. Materials and methods

2.1. Sampling campaigns and sample collection

Two seasonal urban air particulate matter (PM) sampling campaigns, representing different air pollution situations and atmospheric processes were conducted in August (13.–28.08.2013) and October (19.–26.10.2013) in Nanjing, China. The samples were collected separately at day and night at the Nanjing University Xianlin Campus ($32^{\circ} 7' 9.4836''$ N, $118^{\circ} 56' 55.2192''$ E), an urban background location, approximately 18 km northeast of downtown Nanjing. There are several industrial areas in the Nanjing area, including metallurgical and chemical industries, which are mainly to the north, west and southwest of our sample collection site (Wang et al., 2016; Yuan et al., 2017). The location of the sampling site in Nanjing is illustrated in Fig. 1 along with notable local industrial areas and downtown Nanjing, as well as fire maps during the air mass trajectory analyses of August and October campaigns. Fire maps were acquired from LANCE FIRMS MODIS Collection 5 NRT Hotspot/Active Fire Detections MCD14DL, operated by the NASA/GSFC/Earth Science Data and Information System (ESDIS) with funding provided by NASA/HQ (available on-line [<https://earthdata.nasa.gov/firms>]; <https://doi.org/10.5067/FIRMS/MODIS/MCD14DL.NRT.005>). The Xianlin Campus site is generally upwind from downtown Nanjing, but downwind of the densely populated and intensively developed mid-YRD regions including Shanghai and the Suzhou-Wuxi-Changzhou city cluster (Ding et al., 2013).

The PM sampling was conducted using a modified Harvard High Volume Cascade Impactor (HVCI) (Jalava et al., 2006; Sillanpää et al., 2003) as described in detail by Jalava et al. (2015). PM was size-segregated into four fractions according to their aerodynamic diameter: $\text{PM}_{10-2.5}$ ($10\text{--}2.5 \mu\text{m}$), $\text{PM}_{2.5-1.0}$ ($2.5\text{--}1.0 \mu\text{m}$), $\text{PM}_{1.0-0.2}$ ($1.0\text{--}0.2 \mu\text{m}$) and $\text{PM}_{0.2}$ ($<0.2 \mu\text{m}$) particles. $\text{PM}_{10-2.5}$, $\text{PM}_{2.5-1.0}$ and $\text{PM}_{1.0-0.2}$ samples were

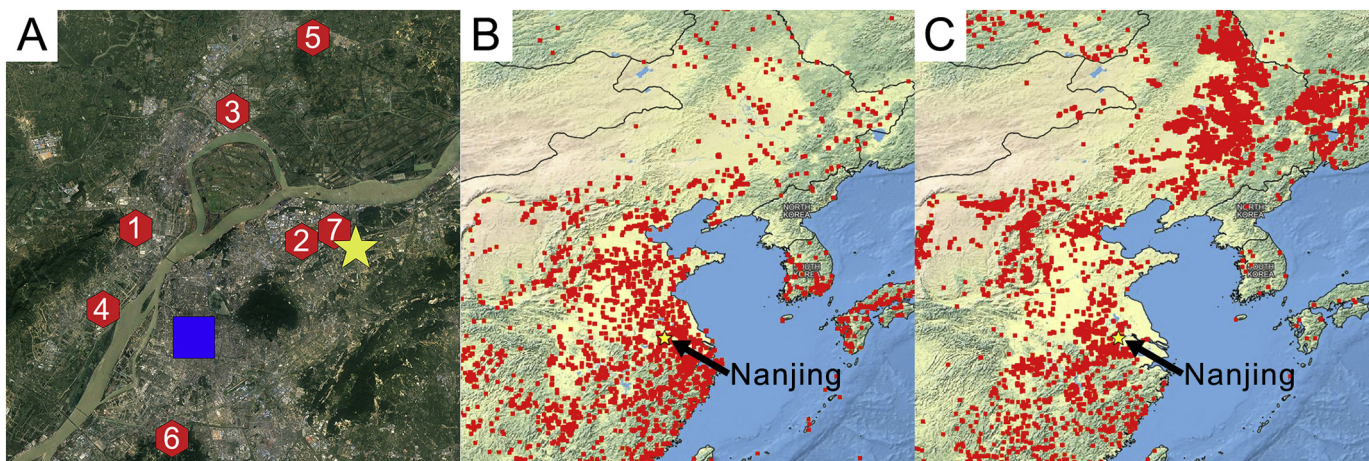


Fig. 1. A) Location of sampling site (star) relative to downtown Nanjing (blue square) and notable local industrial areas (red hexagons). 1 Nanjing High-Tech Industry Development Zone (HTIDZ), 2 Nanjing Economic and Technical Development Zone (ETDZ), 3 Nanjing Chemical Industry Park (CIP), 4 Pukou Economic Development Zone (EDZ), 5 Luhe EDZ, 6 Yuhua EDZ, 7 Qixia EDZ. B and C) Open fires in Eastern and Northeastern China during the air mass trajectory analyses in August (B, 8.8.-28.8.2013), and October (C, 13.10.-26.10.2013), red dots denote open fires.

collected on polyurethane foam (PUF) substrates, and $\text{PM}_{0.2}$ samples were collected on pre-washed polytetrafluoroethylene (PTFE, Fluoropore 3.0 μm FSLW) backup filters. Three field blank filter sets for each campaign were prepared, representing negative control samples in toxicological analyses. The procedure for the preparation of the collected PM samples for chemical and toxicological analyses has been described previously (Jalava et al., 2015; Tapanainen et al., 2012). Briefly, the PM was extracted from the filters in methanol by sonication at temperature below 35 °C, concentrated by rotary evaporation, and dried under nitrogen flow. The achieved extraction efficiencies were >90% for $\text{PM}_{10-2.5}$, >95% for $\text{PM}_{2.5-1.0}$, >96% for $\text{PM}_{1.0-0.2}$, and >90% for $\text{PM}_{0.2}$, calculated by weighing the filters before and after the extraction.

2.2. Meteorological parameters and air mass back trajectory analysis

Ambient temperature, pressure, and relative humidity, as well as wind speed and direction and rainfall were measured with a Vaisala Model WXT520 weather station (WXT) as described by Jalava et al. (2015). The WXT was located 2 m above the measurement container roof. The temperature and relative humidity sensors of WXT are inside a radiation shield, which also protects the sensors from direct exposure to rain. The meteorological data were monitored continuously and later averaged over 1 min and 1 h intervals.

Some gaseous air pollutants (SO_2 , H_2S , NO , NO_2 , NH_3 , O_3) and particle concentrations in two size classes (PM_{10} and $\text{PM}_{2.5}$) were monitored at the same site as described by Jalava et al. (2015). The data were obtained with a 1-minute time resolution and averaged later over 1-hour time resolution.

Backward air mass trajectories were calculated with the HYSPLIT model (Stein et al., 2015; Draxler, 1999; Draxler and Hess, 1998; Draxler and Hess, 1997) for the preceding 5 days (120h) with a 1-hour time resolution. We divided the surroundings into five sectors as shown in Fig. 2: 1) "Northeastern China and Yellow Sea" (main trajectory sector between 0 and 90°), 2) "East China Sea and Shanghai" (90–135°), 3) "Southern China" (135–225°), 4) "Southwestern China" (225–270°), and 5) "Northwestern China" (270–360°). The air masses from the sectors 1, 2, and 3 are assumably a mixture of marine and continental air. Sector 1 includes parts of the Northeastern China, the Korean peninsula, and Japan. Sector 2 is mostly marine, but those air masses cross the highly polluted mid-YRD region including Shanghai and the Suzhou-Wuxi-Changzhou city cluster. Sector 3 is a mixture of marine aerosol and the Southern megacities such as the Guangzhou-Shenzhen-Hong Kong region. The air masses from sectors 4 and 5 are completely continental. We divided the continental sector to

Southwestern and Northwestern China based on differences on annual temperature distribution: in the Northern part houses are heated during wintertime whereas in the Southern part heating is not as extensive.

2.3. Cell culture and PM exposure

The human adenocarcinomic alveolar epithelial cell line A549 (ATCC, CCL-185), a model of type 2 pneumocytes, was used to assess the toxicological effects of the collected PM samples. Cells were maintained in Dulbecco's Modified Eagle Medium (DMEM) supplemented with 10% fetal bovine serum (FBS), 2 mM L-glutamine and 100 U/ml penicillin/streptomycin. All cell culture and exposure reagents were purchased from Sigma-Aldrich unless stated otherwise.

Cells were seeded on 12-well plates (Costar, Corning, NY USA) at 150000 cells/ml/well and cultured for 24 h. One hour prior to the exposure, the culture medium was replaced. The PM samples were reconstituted in 10% dimethyl sulfoxide (DMSO, final concentration 0.05–0.6% v/v in culture medium depending on PM dose) in embryo-transfer water (W1503) under sonication (30 min, below +35 °C). The cells were exposed to five concentrations (25 $\mu\text{g}/\text{ml}$, 75 $\mu\text{g}/\text{ml}$,

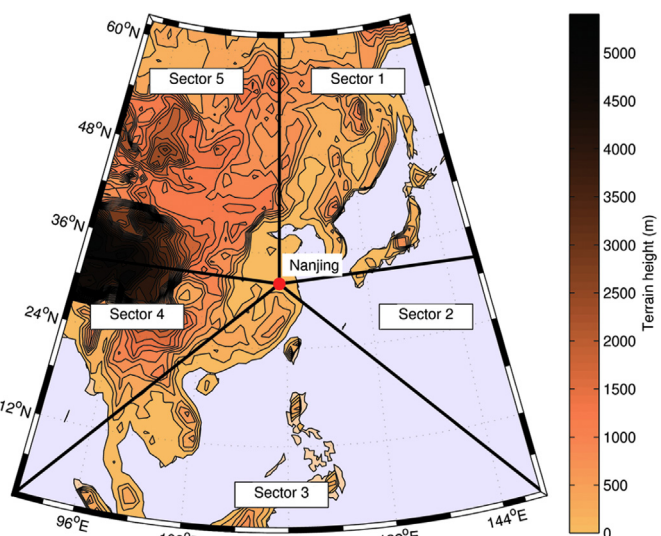


Fig. 2. Designated sectors for air mass back trajectory analysis. Sector 1: "Northeastern China and Yellow Sea", Sector 2: "East China sea and Shanghai", Sector 3: "Southern China", Sector 4: "Southwestern China", Sector 5: "Northwestern China".

150 µg/ml, 200 and 300 µg/ml) of each PM sample, in duplicate, for 24 h at +37 °C, 5% CO₂. After the exposure, the cell culture medium was salvaged and frozen at –80 °C for cytokine analysis. The cells were washed with 1 ml phosphate buffered saline (PBS) and detached by trypsinization (1 ml trypsin-ethylenediaminetetraacetic acid (EDTA) per well, 5-minute incubation at +37 °C, 5% CO₂), followed by the addition of 0.1 ml FBS to stop trypsin activity. The cellular metabolic activity (CMA) was analyzed by 3-(4,5-dimethylthiazol-2-yl)-2,5-diphenyltetrazolium bromide (MTT) assay of two 100 µl aliquots from each duplicate. Cell membrane integrity was analyzed by propidium iodide (PI) exclusion assay, and intracellular oxidative stress by 2',7'-dichlorofluorescein (DCF) assay of a 200 µl aliquot of the duplicates. A 600 µl aliquot of one of the two duplicates was fixed in 70% ethanol and stored at +4 °C for cell cycle analysis, and a 100 µl aliquot of the other of the two duplicates was analyzed for genotoxicity using Single Cell Gel Electrophoresis (SCGE) assay. Each exposure experiment was performed four times. Untreated control cells, filter blank samples corresponding to 150 µg/ml PM dose in volume, and method-specific controls were treated similar to PM samples at each step.

2.4. Toxicological analyses

Cellular metabolic activity, oxidative stress, cell membrane integrity and genotoxicity were measured as described by Kasurinen et al. (2017). We chose the median amount of DNA in the tail as the parameter to estimate genotoxicity using SCGE assay, based on recommendations by Duez et al. (2003); Sunjog et al. (2013). The medians of the four repeated, independent experiments were averaged and the acquired averaged median used as the reported parameter.

IL-8/CXCL8 level was analyzed using enzyme-linked immunosorbent assay (ELISA) kit (R&D Systems, Abington, UK) on 96-well plates (Nunc Maxisorp), according to the manufacturer's instructions with the following exceptions: IL-8 standards were prepared in Reagent Diluent (0.1% bovine serum albumin, 0.05% Tween 20 in Tris-buffered saline (20 mM Trizma base, 150 mM NaCl in deionized water), pH 7.2–7.4, 0.2 µm filtered) in concentrations of 0, 18.8, 37.5, 75, 150, 300 and 600 pg/ml; Streptavidin-Horse Radish Peroxidase (HRP) conjugate solution was diluted to 1% v/v in Reagent Diluent to avoid signal saturation. 3,3',5,5'-tetramethylbenzidine (TMB, Life Technologies, Frederick, MD, USA) was used as substrate. Absorbance was recorded at 450 nm.

Cell cycle phase distribution was analyzed from cells fixed in 70% ethanol. The cells were centrifuged (480 g, 5 min, +4 °C) and ethanol was removed. Cell pellets were washed with 1 ml cold PBS, and then resuspended in 500 µl cold PBS. 7.5 µl RNase A (10 mg/ml) was added to each tube and samples were incubated at +50 °C for one hour, followed by the addition of 4 µl propidium-iodide (1 mg/ml) and incubation at +37 °C for 30 min. Flow cytometric analysis of the cell cycle was carried out using BD FACSCanto™ II (BD Biosciences, San Jose, CA USA).

2.5. PM composition

2.5.1. Inorganic elements and ions

Inorganic elements (Li, Be, B, Na, Mg, Al, K, Ca, Ti, V, Cr, Mn, Fe, Co, Ni, Cu, Zn, As, Se, Rb, Sr, Mo, Ag, Cd, Sb, Ba, Tl, Pb, Bi, Th, U) were analyzed by inductively coupled plasma mass spectrometer (ICP-MS, Agilent Technologies 7700) according to standard EN ISO 17294-2. The samples were first eluted with HNO₃ and HF, then heated within 20 min to +190 °C and kept at this temperature for 20 min. The detection limits were 0.005 µg (Be, B, V, Cr, Co, Ni, Cu, As, Se, Rb, Sr, Mo, Cd, Sb, Ba, Tl, Pb, Bi, Th and U), 0.025 µg (Li, Al, Ti, Mn, Zn and Ag), 0.075 µg (Fe), 0.25 µg (Mg and Ca) and 1 µg (Na and K).

Anions (Br[−], Cl[−], NO₃[−], SO₄^{2−}, F[−], PO₄^{3−}) were analyzed with ion chromatography (IC, Metrohm Compact 882 ICplus with column Metrosep a SUPP5-150/4.0) according to standard EN ISO 10304-1/2. The samples were prepared by eluting with NaOH and Na₂CO₃ in an ultrasonic

treatment. The detection limits were 1 µg (Br[−], Cl[−], NO₃[−], SO₄^{2−}, PO₄^{3−}) and 2 µg (F[−]).

2.5.2. Polycyclic aromatic hydrocarbons

A total of 30 unsubstituted and alkylated polycyclic aromatic hydrocarbons (PAH) were analyzed by using a gas chromatograph mass spectrometer (6890N GC, equipped with 5973 inert Mass Selective Detector, Agilent Technologies). HP-17-MS column was used for the separation of the compounds. The equipment was operated with selected ion monitoring (SIM) mode. The analysis was carried out as described in Sippula et al. (2013). The detection limit of the method was 0.1 ng/mg. The sum of the known genotoxic PAH compounds were calculated according to (World Health Organization, International Programme on Chemical Safety, 1998).

For analysis of selected PAH and oxygenated PAH extraction was carried out with dichloromethane (GC ultra-grade, Roth, Germany) in an ultrasonic bath. Prior to extraction approximately 1.5 mg samples were spiked with internal standard mixtures. Sonication was carried out three times, each with 500 µl of solvent for fifteen minutes. The three extracts were combined and filtered over PTFE syringe membrane filters (0.2 µm, Sartorius, Germany) and finally the volume was reduced to 100 µl. Samples were directly injected to the GC-MS-System (Shimadzu GCMS-QP2010 Ultra, Shimadzu, Japan), which was equipped with a 30 m BPX-5 column from SGE (0.22 mm ID, 0.25 µm film, SGE, Australia). A calibration was done by using the same set of internal standards and procedures (except sonication and filtration). Relative Standard Deviations of the procedure were calculated via the confidence intervals.

2.6. Statistical analyses

Levene's test was used to test for homogeneity of variance. In the case of equal variances, comparisons of samples vs. single control were performed by one-way ANOVA followed by Dunnett's two-sided post-hoc test, and in the case of unequal variances by Welch's F-test followed by Dunnett's T3 post-hoc test. For pairwise comparisons between samples, one-way ANOVA followed by Tukey's HSD test was performed when variances were equal; in the case of unequal variances, Dunnett's T3 post-hoc test was used. For SCGE assay, statistical analysis was performed by the nonparametric Jonckheere-Terpstra test for ordered alternatives, as suggested by Duez et al. (2003). Spearman's ρ correlation was run to determine the correlations between observed cellular responses at different endpoint analyses and the measured chemical components in PM samples. The results of the statistical tests were considered significant when *p* < 0.05. Statistical analyses were performed using IBM SPSS version 23.

3. Results

3.1. Sample collection, atmospheric and meteorological conditions, and air quality

Fig. 3 illustrates the variations of calculated PM concentrations in air during the two sampling campaigns, based on the collected sample masses by HVCI. The observed PM concentrations were higher during October compared to August in all size ranges. In August, all size-segregated samples showed lower average mass concentrations at night than in the daytime, whereas in October virtually no difference in average mass concentrations between day and night were observed, but variations were present between samplings (Supplementary Table S1). The highest concentrations were seen for October PM_{10–2.5}, twice higher than August during the daytime samplings, and over three times higher than August for nighttime samplings. PM_{2.5–1.0} concentrations were very similar for day and night during both campaigns, but much higher in October than August. PM_{1.0–0.2} concentrations were higher than PM_{2.5–1.0}, with highest concentrations during daytime August and at

night in October. The variation in concentrations between sampling campaigns was the lowest for $\text{PM}_{0.2}$. Day-night variation was the greatest for August $\text{PM}_{10-2.5}$ samples, and relatively large for August $\text{PM}_{0.2}$. In October, day-night variation was very low.

A summary of sampling durations, meteorological parameters (temperature, relative humidity, atmospheric pressure, wind speed and direction, rainfall, and solar irradiation) and the results of continuous air quality measurements for daytime and nighttime samplings are displayed in Table 1. In Table 2, we present an overview of the corresponding air mass back trajectory analyses. These data for the individual sample collections are available in (Supplementary Table S2). As shown in Table 1, the average hourly temperatures in August were clearly higher in comparison with October during both day and nighttime. During both campaigns, the daytime average temperature was slightly higher than night. The relative humidity was higher during nighttime than during daytime. The average atmospheric pressure was lower during the August campaign compared to October. Furthermore, the rainfall during the August campaign, of which approx. 75% were accumulated during daytime mainly during two days, and the rest mainly during one night, whereas there was no rainfall in Nanjing during the October. In addition, the average time after last rainfall before the air masses entered the measurement site was 34 h during the August campaign, and 86 h during the October campaign. These findings highlight the different weather types and aerosol age for the campaigns.

During both sampling campaigns, the wind speeds were lower during the stable conditions at night than during the turbulent conditions in the day; correspondingly, the percentages of calm weather (defined as wind speed below 1.0 m/s) were higher during nighttime when compared to day. In August, the daily average PM concentration rose from the minimum at ca. 04:00 towards the maximum at 20:00, whereas in October, the lowest PM concentration was observed at ca. 10:00 and the maximum was reached at 22:00 (data not shown). The monitored gaseous pollutants display day-night variations; SO_2 , mainly emitted in oil refining and high temperature combustion processes, and O_3 levels were higher during the day, whereas H_2S and NO_2 showed elevated levels at night. Unlike the other gaseous pollutants in our data, NH_3 showed different profiles of daily average concentrations depending on the sampling campaign. In August, NH_3 concentration displayed a sharp daytime increase starting at ca. 8:00 in the morning and reaching its peak at ca. 11:00–14:00; the profile appeared to follow the solar irradiance and O_3 levels. On the other hand, in October the NH_3 peak concentration was reached at ca. 8:00 in the morning after a slow accumulation through the night, and the concentration dropped sharply to its minimum at ca. 16:00 displaying an inverse relationship with solar irradiance and O_3 .

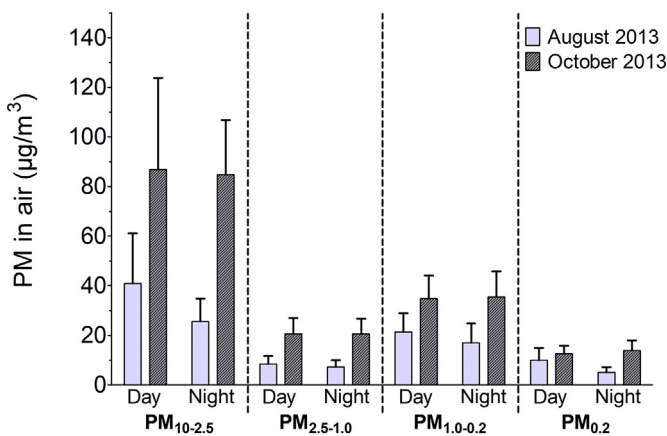


Fig. 3. Calculated average size-segregated PM concentrations in air during day- and nighttime sample collections in August and October. Error bars represent standard deviation.

Table 1

Summary of sampling durations, local weather conditions in Nanjing, and the results of continuous, separate air quality measurements during sample collection. Averaged results.

Parameter	August		October	
	Day	Night	Day	Night
Sampling duration (h)	124.6	203.6	215.2	348.2
T (°C)	31.8	28.9	18.6	14.7
RH (%)	60.0	72.1	48.3	64.5
p (mbar)	999.8	999.8	1017.7	1017.9
Wind direction (°)	89.4	91.0	23.3	72.1
Wind speed (m/s)	2.9	2.2	2.1	1.2
Rain (mm)	60.4	20.7	0.0	0.0
Solar irradiance (W/m²)	451.6	25.1	443.9	5.7
Calm (% of time)	10.1	19.7	23.4	58.1
SO_2 (ppb)	6.0	5.2	10.0	8.4
H_2S (ppb)	0.9	1.3	1.0	2.3
NO (ppb)	4.5	3.9	7.0	37.4
NO_2 (ppb)	9.1	12.5	13.0	25.4
NH_3 (ppb)	30.8	16.2	11.9	13.8
O_3 (ppb)	56.3	27.2	47.2	12.8
PM_{10} ($\mu\text{g}/\text{m}^3$)	78.3	78.5	120.3	212.7
$\text{PM}_{2.5}$ ($\mu\text{g}/\text{m}^3$)	38.4	35.3	65.3	92.7
$\text{PM}_{10-2.5}$ ($\mu\text{g}/\text{m}^3$)	39.9	43.2	55.1	120.0
$\text{PM}_{2.5}/\text{PM}_{10}$	0.49	0.45	0.54	0.44

The prevailing wind directions were Northeast and East during the August campaign and North during the October campaign (Fig. 4). According to the air mass backward trajectory analysis (Table 2), during the August campaign the air masses originated mostly from the marine areas (Sector 1: 36.7%, Sector 2: 24.2%, Sector 3: 32.5%, Sector 4: 0.0%, Sector 5: 6.6%; on average, 54 h over sea), whereas during the October campaign the air masses were more of continental origin (Sector 1: 63.7%, Sector 2: 2.1%, Sector 3: 2.7%, Sector 4: 0.0%, Sector 5: 31.5%; on average, 23 h over sea). It is worth noting that the Sector 4 was not represented at all in either campaign, removing the emission contributions from downtown and southwestern Nanjing as well as Southwestern China from the collected PM samples. This is in accordance with the wind directions: the wind sector from Southwest to West has a very low frequency in both campaigns (Fig. 4). The wind direction patterns are quite similar during the daytime and nighttime during the August campaign, whereas during the October campaign they differ distinctly: during the daytime the wind blows mainly from North, whereas during the nighttime the wind directions are distributed almost evenly between North and South. The air quality data (TEOM, Table 1) shows that both the PM_{10} and $\text{PM}_{2.5}$ concentrations are higher during the nighttime. The air mass origins display no large differences between the daytime and nighttime fractions of the air mass sectors. As shown in Fig. 5, in August the Northern air masses (Sectors 1 and 5) had encountered no recent rainfalls, whereas in Sectors 2 and 3 the rainfalls

Table 2

Summary of air mass trajectory analysis showing the percentage of time air masses had spent in each sector, in or above mixing layer, or over sea. Averaged results.

Parameter	August		October	
	Day	Night	Day	Night
Main sector	1	1	1	1
Sector1 (%)	34.3	38.1	60.7	65.5
Sector2 (%)	25.6	23.3	2.1	2.0
Sector3 (%)	33.0	32.3	4.0	1.9
Sector4 (%)	0.0	0.0	0.0	0.0
Sector5 (%)	7.2	6.3	33.1	30.6
Height above sea level (m)	336.3	358.0	821.2	832.5
Height above ground level (m)	234.6	255.4	532.8	547.1
Mixing depth at measurement site (m)	780.6	371.9	808.5	228.2
In mixing layer (%)	87.6	84.8	66.7	67.9
Above mixing layer (%)	12.4	15.2	33.3	32.1
Time after last rainfall (h)	28.8	37.2	84.4	86.8
Over sea (%)	54.5	53.4	22.7	23.1
Time after last sea touch (h)	20.1	17.5	17.5	17.4

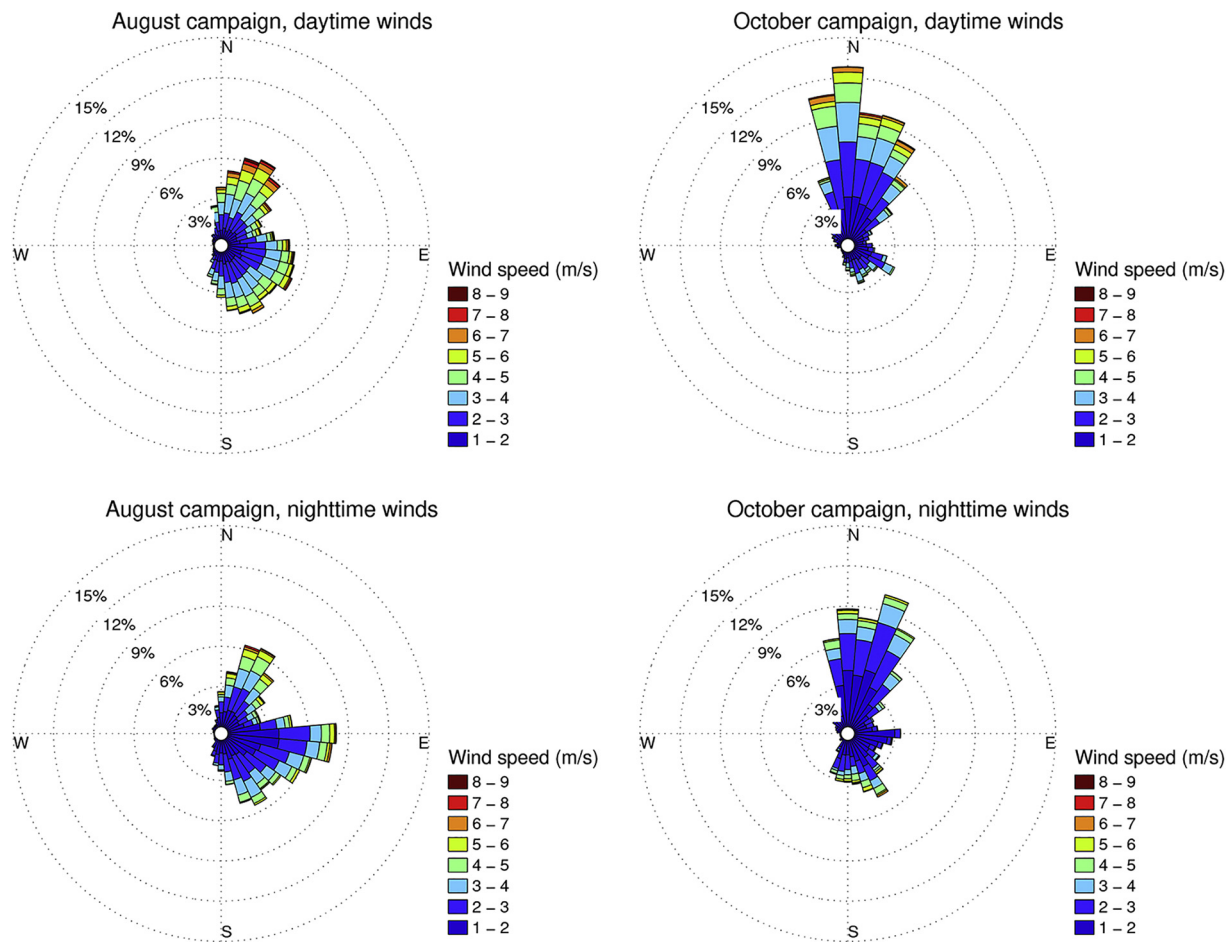


Fig. 4. Wind distribution for the August campaign (left) and the October campaign (right).

were quite recent and occurred shortly before the air masses crossed the YRD region. This removes some of the pollutant contributions, especially in PM_{10-2.5} fraction, from distant sources from Sectors 2 and 3 while emphasizing the regional emissions of YRD region, which contained a large amount of open fire activity in August as depicted in Fig. 1.

The average mixing depth was higher (524 m) during the August campaign than during the October campaign (446 m). Naturally, there is a strong diurnal variation in the mixing depth (Table 2). The time fractions that the air masses spent during the last 5 days in the mixed layer were 85.9% and 67.5% in the August and October campaigns,

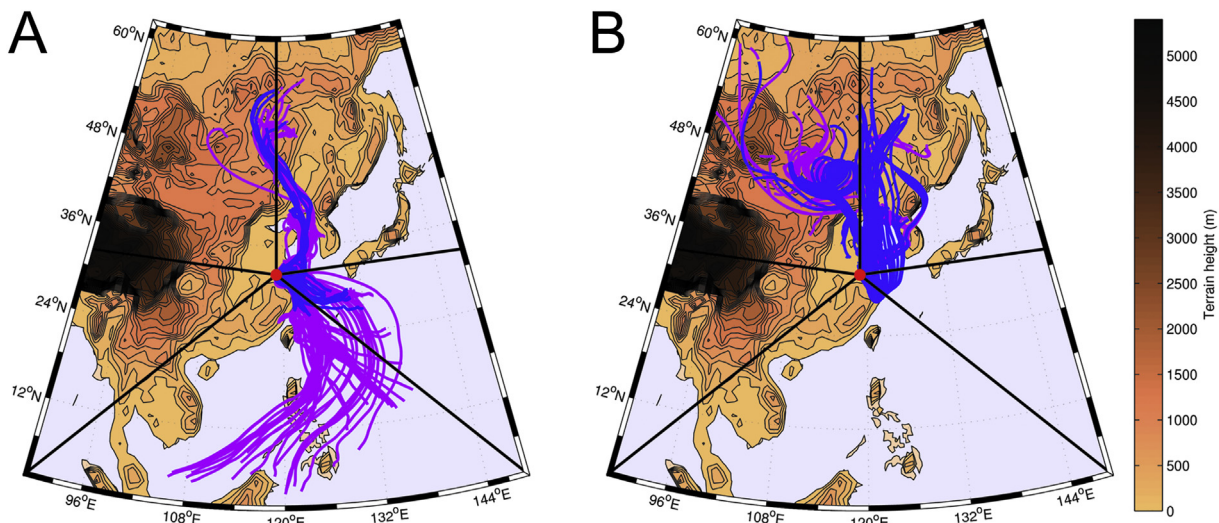


Fig. 5. Air mass trajectories during August (A) and October (B) sampling campaigns. Purple trajectories denote air mass movements with no rainfall, blue trajectories denote air mass movements after the last rainfall on the trajectory, red dot depicts Nanjing, and the black lines depict sector borders for trajectory analysis.

respectively. This is evident, because the corresponding average heights of the incoming air masses during the last 5 days were 350 m and 828 m.

3.2. Chemical composition

The recorded masses of PM constituents correspond to 46–47% of PM mass for $\text{PM}_{10-2.5}$, 38–59% for $\text{PM}_{2.5-1.0}$, 52–86% for $\text{PM}_{1.0-0.2}$ and 45–53% for $\text{PM}_{0.2}$; thus, roughly half of PM mass is comprised of material not quantified by our analyses, such as elemental/black carbon, unanalyzed species of organic carbon, and biogenic material. For $\text{PM}_{1.0-0.2}$ the quantified PM constituents amount to 73–86% of total PM mass in the October samples, differing significantly from the August samples where the measured components contribute to 52–55% of PM mass. In $\text{PM}_{0.2}$, this difference is smaller, 53% in October vs. 45–46% in August samples, while there is no such difference in $\text{PM}_{10-2.5}$ or $\text{PM}_{2.5-1.0}$.

3.2.1. Inorganic elements and ions

The amounts of inorganic elements and ions in PM samples displayed great variability, as shown in Table 3 (extensive tabulation of all measured chemical constituents can be found in the Supplementary Table S3). Distinct differences between PM size ranges, sampling campaigns, and day and night were readily visible for several of the displayed constituents. Elemental Al, Ca, Fe, Mg and Na were most abundant in $\text{PM}_{10-2.5}$ and $\text{PM}_{2.5-1.0}$. Al, Ca and Fe exhibited higher concentrations in October samples compared to August; Ca concentration was also highest at night except for August $\text{PM}_{10-2.5}$. Furthermore, K was more abundant in October than August samples in all size ranges, whereas Na displayed higher concentrations in August. Cl^- was most abundant in $\text{PM}_{10-2.5}$ and $\text{PM}_{2.5-1.0}$ with a notable presence in $\text{PM}_{1.0-0.2}$ but displayed very low concentrations in $\text{PM}_{0.2}$. Cd, Cu, K, Pb, and secondary inorganic ion SO_4^{2-} exhibited lower concentrations in the larger size ranges and relatively higher concentrations in $\text{PM}_{1.0-0.2}$ and $\text{PM}_{0.2}$. NO_3^- was abundant in all size ranges. Mass fractions of some constituents, such as Cu and Cl^- , showed clear differences between sampling campaigns or day and night in only certain size ranges; Cu exhibited higher concentrations in August $\text{PM}_{2.5-1.0}$ and $\text{PM}_{0.2}$ in comparison with October. Moreover, SO_4^{2-} displayed higher concentrations at night in August for $\text{PM}_{10-2.5}$ and $\text{PM}_{2.5-1.0}$, but otherwise was more abundant in the daytime samples.

3.2.2. PAH compounds

Concentrations of PAH compounds in the PM samples displayed variations between size ranges, sampling campaigns, and day and night, as can be seen in Table 4. $\text{PM}_{2.5}$ contained 79–83% of all measured PAHs, including oxygenated PAHs (OPAHs). The total amounts of PAHs were the greatest in $\text{PM}_{2.5-1.0}$ and $\text{PM}_{1.0-0.2}$ fractions, which contributed to 28–39 and 25–33% of total mass of PAHs in the total PM_{10} mixture, respectively. The contributions to total PAH mass were 11–24% for $\text{PM}_{0.2}$ and 17–21% for $\text{PM}_{10-2.5}$. Unsubstituted and alkylated PAHs and genotoxic PAHs were most abundant in the three smallest size ranges but displayed notable levels in $\text{PM}_{10-2.5}$ as well. Genotoxic PAHs constituted 78–81% of all PAHs in $\text{PM}_{0.2}$, and the greatest genotoxic PAH concentration was observed for the October Night $\text{PM}_{0.2}$ sample. Oxygenated PAHs (OPAHs) displayed high concentrations primarily in $\text{PM}_{2.5-1.0}$ and $\text{PM}_{1.0-0.2}$, with again notable amounts in $\text{PM}_{10-2.5}$, but extremely low concentration in $\text{PM}_{0.2}$.

Overall, PAH concentrations were clearly higher at night for both sampling campaigns. The amounts of unsubstituted, alkylated, and genotoxic PAHs for $\text{PM}_{10-2.5}$ were higher in August, whereas in the other size ranges these concentrations were higher in October. OPAH concentrations were drastically higher in October for $\text{PM}_{10-2.5}$, but higher in August for $\text{PM}_{2.5-1.0}$ and $\text{PM}_{1.0-0.2}$. Fluoranthene, pyrene, and their alkyl derivatives, as well as phenanthrene and chrysene were generally the most abundant unsubstituted and alkylated PAHs, jointly contributing to 70–85% of unsubstituted and alkylated PAHs and 28–74% of all PAHs in the samples (Supplementary Table S3). Benzo[a]pyrene and benzo[k]fluoranthene demonstrated the distribution of genotoxic PAHs between the size range with low concentrations in $\text{PM}_{10-2.5}$ and relatively much higher amounts in $\text{PM}_{2.5}$. The OPAHs 9H-fluoren-9-one, xanthone, 9,10-anthracenedione and 1,8-naphthalic anhydride demonstrate the high variability of OPAH concentrations both between size ranges and between the four samples within each size range. These four OPAHs comprised the bulk of measured total OPAH concentrations when they were present in any given sample, and in these samples contributed greatly to the total PAH concentration. Picene and retene were present at low concentrations in most samples, whereas the four OPAHs displayed either not detected or very low concentrations in most samples, but very high concentrations in certain samples. Of these OPAHs, 9,10-anthracenedione was detected in most of the samples, albeit in relatively low concentrations. In contrast, 9H-fluorenone was present in very high concentrations in only October Night $\text{PM}_{10-2.5}$, and both October $\text{PM}_{2.5-1.0}$ samples. High concentrations of xanthone were recorded

Table 3

Mass concentrations ($\mu\text{g}/\text{mg}$ PM mass) of select inorganic ions and elements in size-segregated PM samples.

	$\text{PM}_{10-2.5}$		$\text{PM}_{2.5-1.0}$		$\text{PM}_{1.0-0.2}$		$\text{PM}_{0.2}$					
	August		October		August		October		August		October	
	Day	Night	Day	Night	Day	Night	Day	Night	Day	Night	Day	Night
Total inorganics	461.81	470.52	466.07	472.59	422.33	563.78	591.94	381.73	524.12	549.59	858.24	732.84
Al	46.07	36.29	61.72	61.35	13.12	10.25	19.11	23.73	1.48	3.29	4.32	3.59
As	n.d.	0.03	n.d.	n.d.	0.02	0.06	0.01	n.d.	0.10	0.09	0.02	0.05
Ca	109.34	86.38	135.56	191.93	27.62	34.15	34.63	45.84	8.68	8.35	10.44	7.60
Cd	0.01	0.01	0.02	0.01	0.02	0.02	0.03	0.03	0.03	0.02	0.02	0.02
Cr	0.22	0.18	0.17	0.16	0.23	0.32	0.14	0.20	0.11	0.14	0.06	0.11
Cu	0.23	0.25	0.16	0.20	0.74	0.72	0.29	0.40	0.46	0.34	0.39	0.51
Fe	26.71	23.63	36.33	36.20	7.59	7.96	10.94	16.68	1.22	2.03	0.31	6.42
K	8.14	6.98	12.01	12.77	5.41	7.80	15.58	19.60	9.48	7.10	22.03	28.49
Mg	8.20	6.26	9.85	8.40	3.51	3.08	2.77	3.59	n.d.	n.d.	n.d.	0.28
Mn	0.77	0.63	1.01	1.06	0.73	0.79	0.83	1.31	0.66	0.57	1.19	1.40
Na	19.19	19.27	4.36	n.d.	17.96	14.57	3.10	2.79	1.42	2.99	n.d.	10.82
Ni	0.16	0.11	0.13	0.14	0.15	0.13	0.10	0.14	0.15	0.10	0.15	0.10
Pb	0.59	0.36	0.49	0.43	0.85	1.02	1.19	1.36	1.52	1.25	1.49	1.63
Zn	3.57	4.77	2.77	4.17	7.89	9.35	9.13	12.58	4.80	4.07	5.47	6.09
Cl^-	22.16	39.24	17.86	14.33	14.16	29.09	20.00	27.00	2.91	11.32	21.56	24.34
SO_4^{2-}	32.84	58.48	42.90	41.28	174.75	222.46	242.57	1.87	426.02	339.66	445.56	355.56
NO_3^-	177.78	181.29	133.59	93.29	146.04	219.79	229.73	222.00	64.29	167.24	344.44	295.96

Bold numbers indicate maximal values within the four samples in each size range. n.d. = not detected.

Table 4

Mass concentrations (ng/mg PM mass) of select PAH compounds in size-segregated PM.

	PM _{10-2.5}				PM _{2.5-1.0}				PM _{1.0-0.2}				PM _{0.2}			
	August		October		August		October		August		October		August		October	
	Day	Night	Day	Night	Day	Night	Day	Night	Day	Night	Day	Night	Day	Night	Day	Night
Total PAHs and OPAHs	213.43	401.31	204.66	430.00	496.06	753.09	382.76	589.35	416.32	494.26	296.72	655.26	143.47	283.36	284.52	453.26
Unsubstituted and alkylated PAHs	146.55	299.51	85.77	154.85	254.63	412.46	266.65	418.91	191.30	326.36	270.87	418.95	143.47	279.16	275.83	438.92
Genotoxic PAHs	81.80	176.81	53.87	102.12	172.52	281.14	194.32	318.52	125.14	243.84	214.60	336.18	111.76	221.95	230.12	367.28
OPAHs	65.66	99.16	118.89	275.15	241.43	335.97	116.11	170.43	225.02	167.90	25.85	236.31	n.d.	4.20	8.69	14.34
Benz[a]pyrene	3.87	6.00	2.91	6.89	8.82	14.32	12.55	25.12	7.30	16.14	14.37	27.01	6.27	12.44	16.13	29.48
Benz[k]fluoranthene	0.74	8.96	0.61	2.84	5.28	14.37	6.49	6.80	0.67	2.41	15.68	9.82	2.83	3.16	2.18	10.24
Picene	n.d.	2.84	n.d.	1.17	2.91	7.73	4.12	4.44	6.18	1.76	3.16	2.84	n.d.	5.44	2.42	4.61
Retene	1.78	4.85	0.81	1.23	3.35	7.02	1.54	2.23	3.46	1.71	0.85	2.15	n.d.	3.18	0.60	1.43
9H-Fluoren-9-one	2.65	5.67	n.d.	116.00	n.d.	n.d.	87.20	83.70	n.d.	n.d.	n.d.	n.d.	n.d.	n.d.	n.d.	n.d.
Xanthone	n.d.	0.96	112.00	153.00	n.d.	n.d.	n.d.	58.30	n.d.	n.d.	n.d.	n.d.	n.d.	n.d.	n.d.	n.d.
9,10-Anthracenedione	19.30	37.10	6.89	5.92	32.60	55.70	27.40	25.60	40.50	46.90	20.50	25.80	n.d.	7.25	10.90	n.d.
1,8-Naphthalic anhydride	43.50	52.50	n.d.	n.d.	206.00	272.00	n.d.	n.d.	180.00	121.00	n.d.	203.00	n.d.	n.d.	n.d.	n.d.

Bold numbers indicate maximal values within the four samples in each size range. n.d. = not detected.

in October PM_{10-2.5} samples and October Night PM_{2.5-1.0}. 1,8-naphthalic anhydride displayed a clear presence in August samples for PM_{10-2.5}, PM_{2.5-1.0} and PM_{1.0-0.2}, with the only recorded October sample containing it being October Night PM_{1.0-0.2}.

3.3. Toxicological characteristics

3.3.1. Intracellular oxidative potential

As illustrated in Fig. 6, PM_{10-2.5} induced a dose-dependent oxidative stress response in A549 cells, with October Day sample reaching up to 75.8% and October Night up to 85.7% increased responses compared to negative control; yet, no significant differences between August and October were detected. Virtually no response was observed for the lowest

25 µg/ml dose, and 75 µg/ml dose induced increased responses only for October Day and Night samples (12.4% and 14.7% increased responses, respectively). The sub-PM_{2.5} size ranges showed no significant responses, but August Day sample produced generally higher responses than the other samples in these size ranges.

3.3.2. Cytotoxicity

As shown in Fig. 7, all PM samples induced dose-dependent decreases of CMA; the greatest cytotoxic effects were observed for PM_{2.5-1.0} and PM_{0.2}. For PM_{10-2.5}, reduction of CMA reached its peak at 29.8–30.9% for 300 µg/ml dose in all samples; filter blank sample caused 12.6% reduction of CMA, which was roughly equivalent to the response level of the lowest PM dose. PM_{2.5-1.0}-induced reduction of CMA

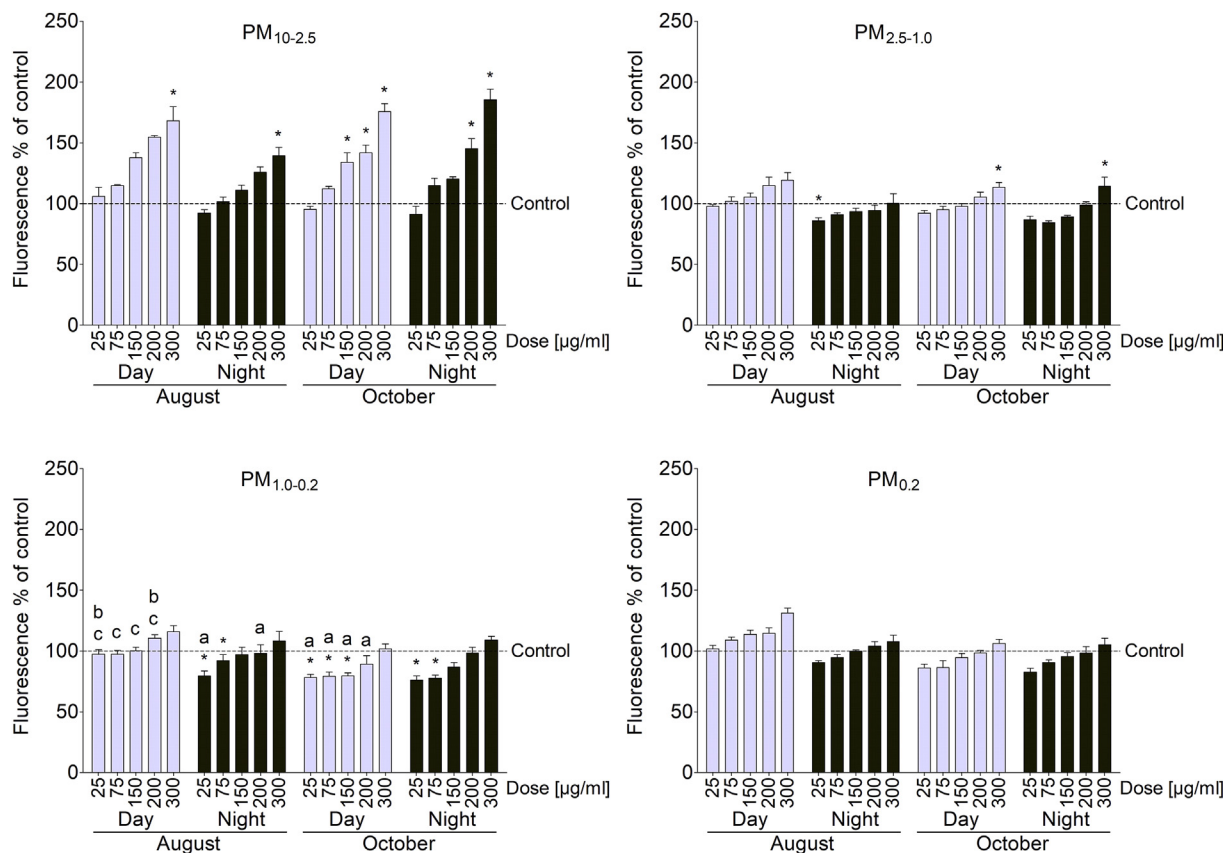


Fig. 6. Intracellular oxidative potential as measured by DCF assay. * denotes a significant ($p < 0.05$) difference to control, letters denote a significant difference to the corresponding dose of another sample (a August Day, b August Night, c October Day, d October Night). Error bars represent SEM, $n = 4$.

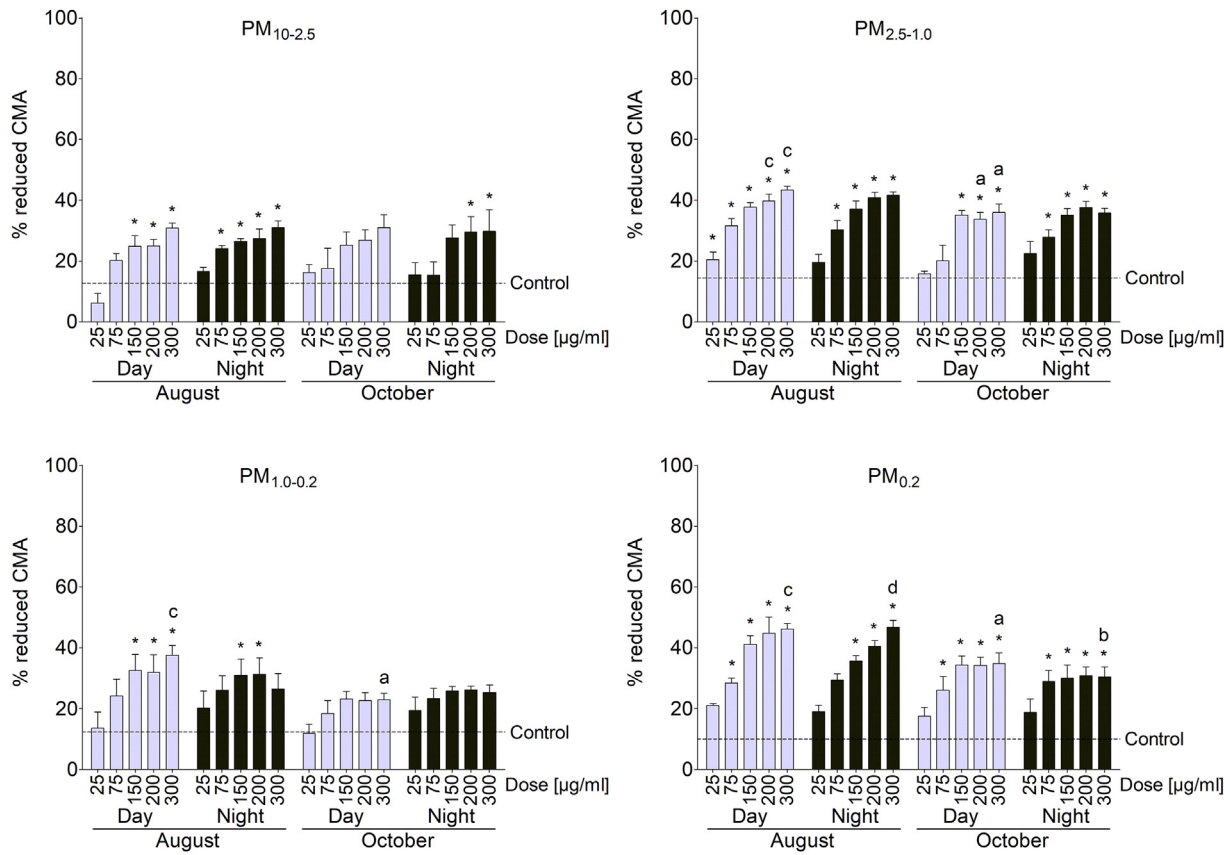


Fig. 7. Reduction of cellular metabolic activity (CMA) compared to untreated control as measured by MTT assay. * denotes a significant ($p < 0.05$) difference to control, letters denote a significant difference to the corresponding dose of another sample (a August Day, b August Night, c October Day, d October Night). Error bars represent SEM, $n = 4$.

reached 41.6–43.4% for the highest dose of August samples, and up to 35.8–35.9% for the corresponding dose of October samples. The responses for the lowest dose were between 15.8 and 22.5% reduced CMA with no significant differences between August and October. On the other hand, significant August–October differences were detected for the two highest doses. PM_{1.0-0.2} produced significant responses for both August samples, up to 37.6% decreased CMA for 300 µg/ml dose of August Day sample and 31.3–32.0% decreases for 200 µg/ml dose of both August samples, with blank control causing 12.4% decreased CMA. In contrast, the October samples induced at most 25.2% reduction of CMA for October Night and 22.9% for October Day, with both reaching a peak response level starting at 150 µg/ml dose. PM_{0.2} August samples showed higher cytotoxic responses than October samples, with August samples causing 46.1–46.7% decreased CMA for the highest dose whereas October samples decreased CMA by 30.4–34.9% at the same dose, and blank control caused 10.0% decreased CMA. The October Night sample reached its peak response level of approx. 30% reduced CMA already for 75 µg/ml dose, and October Day sample showed a stable peak response level of 34–35% for doses 150–300 µg/ml.

Integrity of the cell membrane was measured by propidium iodide (PI) exclusion assay, utilizing a DNA dye unable to freely permeate an intact cell membrane (data not shown). No significant increase of PI-positive, i.e. membrane-compromised, cells were observed for PM_{10-2.5} compared to control. For PM_{2.5-1.0}, the responses ranged from the control level of 2.2% up to 15.5% PI-positive cells. PM_{1.0-0.2} samples displayed significant increases of PI-positive cells from control level of 6.9% up to 22.7%, but no clear pattern was observed. Except the October Night sample, all PM_{0.2} samples induced significant increases of PI-positive cells starting from 75 or 150 µg/ml doses, ranging from 6.0% up to 15.0% PI-positive cells.

3.3.3. Genotoxicity

As depicted in Fig. 8, PM_{10-2.5} induced a very strong genotoxic response, especially for the August samples. August Day induced a significant dose-dependent increase of DNA damage with up to 41.1% DNA in tail for the highest dose. August Night did not show a dose-dependently increasing genotoxic response but exhibited 21.8% DNA in tail already for 75 µg/ml dose, with peak response level at 29.0% DNA in tail for 150 and 200 µg/ml doses; the response for the highest dose was lower at 12.5% DNA in tail. October samples produced lower responses, reaching 16.2–17.1% DNA in tail for the highest dose and a dose-dependent increase of DNA in tail for the October Night sample. PM_{2.5-1.0} showed no significant dose-dependent increases of DNA in tail. PM_{1.0-0.2} exhibited significant increases of DNA in tail except for the August Day sample, but the highest observed responses were low at 7.5–9.0% DNA in tail. PM_{0.2} induced significant dose-dependent increases of DNA in tail for the August and October Night samples, with peak response level of 6.4–7.1% DNA in tail. Yet, the greatest responses in this size range were observed for the highest dose of August and October Day samples, which induced 9.4–9.8% DNA in tail.

3.3.4. Cell cycle phase distribution

The recorded percentages of cells in Sub-G1/G0 phase are illustrated in Fig. 9. In PM_{10-2.5}, only the largest dose of August Night sample exhibited a significant increase of Sub-G1/G0 phase population size to 7.7%; Sub-G1/G0 population size for filter blank was 3.1% of all recorded cells.

PM_{2.5-1.0} caused significant cell cycle changes; all samples induced dose-dependent increases of Sub-G1/G0 phase population, with clear differences to filter blank starting from 75 (night samples) and 150 µg/ml doses (day samples). October samples produced the highest

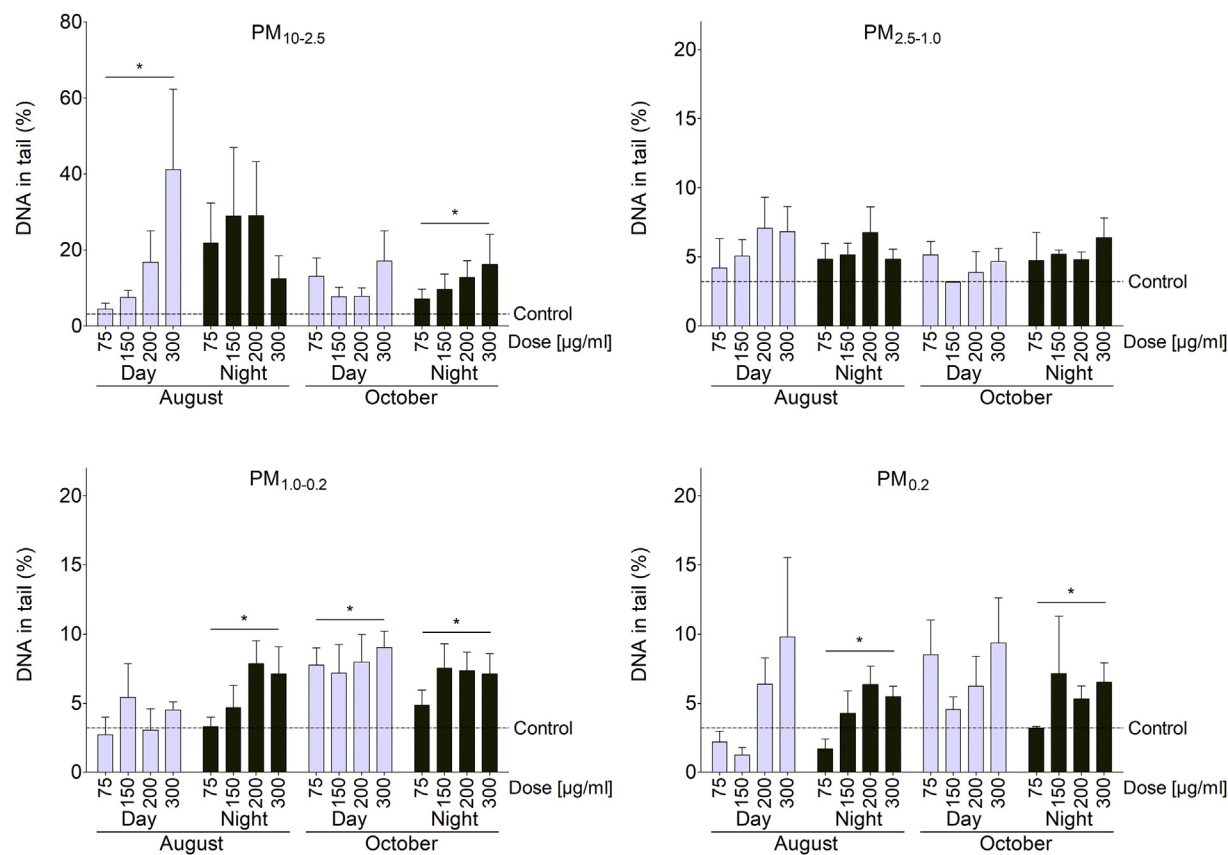


Fig. 8. Genotoxicity as measured by the alkaline SCGE assay, which allows the detection of DNA strand breaks and alkaline labile breaks associated with incomplete excision repair, reported as averaged median percentage of DNA in tail. Capped line with a star indicates a significant ($p < 0.05$) dose-dependent increase of DNA in tail compared to untreated control. Error bars represent SEM, $n = 4$.

responses; October Night sample exhibited 15.1–17.6% cells in Sub-G1/G0 phase for 150–300 µg/ml doses and October Day 9.3–12.4% for the same doses. August Night sample showed 7.8–10.7% and August Day 5.9–8.0% cells in Sub-G1/G0 phase for 150–300 µg/ml doses.

The increase of Sub-G1/G0 population for PM_{1.0-0.2} demonstrated capped responses; the amount of cells in this phase reached its maximum value for 200 µg/ml dose for all samples with a slightly lower response for the largest dose. The greatest response was observed for August Day sample (12.0%), followed by October Night at 11.5%. In contrast to the larger size ranges, the smallest doses of PM_{1.0-0.2} caused significant, yet mild, increases of Sub-G1/G0 population.

The cell cycle effects were greatly pronounced for PM_{0.2}. A significant dose-dependent increase of Sub-G1/G0 population was observed for all samples with the highest responses for October samples; 20.3% cells were in Sub-G1/G0 phase for the highest dose of October Night and 15.6% for October Day. Both October samples also caused significant responses already for the lowest dose (3.9–4.7% cells in Sub-G1/G0 phase). In contrast to October samples, August Day caused a higher response than August Night, 13.9 and 10.6% for the highest dose.

3.3.5. Inflammation - proinflammatory chemokine IL-8/CXCL8

As shown in Fig. 10, the responses for PM_{10-2.5} exhibited a high IL-8 level for the smallest dose for all samples (91.9–120.3% increase compared to untreated control), but the responses were not dose-dependent for August samples and inversely dose-dependent for October samples. The highest IL-8 levels were elicited by August Night sample, which produced 149.0% increased IL-8/CXCL8 concentration for 150 µg/ml dose. October samples elicited their highest responses, 107.5–110.5% increase, for 75 µg/ml dose, but for doses 150–300 µg/ml the increasing dose resulted in decreasing IL-8 concentration. The largest dose

of October samples reduced the IL-8 concentration to only 17.7–20.2% higher than the control level.

Significant dose-dependent increases of IL-8/CXCL8 concentration were detected for August samples in PM_{2.5-1.0} size range, with the highest dose of August Night sample producing the highest IL-8 response, 243.9% increase compared to control, out of all studied samples in all size ranges. August Day sample reached 171.6% increased response for the highest dose, whereas the October samples showed bell-shaped response curves with the responses for the smallest and highest doses at similar levels of 31–47% higher than control level.

The responses for PM_{1.0-0.2} were low in comparison to the other size ranges. August Night sample exhibited dose-dependency with 105.0–107.4% increased IL-8/CXCL8 concentration for 200 and 300 µg/ml doses. August Day and October Night showed shallow bell-shaped response curves in the range of 34.4–67.9% increased concentration, while October Day elicited a slowly declining response-curve with the highest concentration, 58.0% increase over control level, for 25 µg/ml dose and the lowest concentration, 32.5% higher than control level, for 300 µg/ml dose.

In PM_{0.2} size range, August Night sample elicited the greatest dose-dependent inflammatory response, reaching 196.2% increase over control level for 300 µg/ml dose. August Day and October Night showed also dose-dependently increasing response-curves with the highest concentrations at 94.1% and 118% higher than control level. The highest response for October Day, 82.6% increased IL-8/CXCL8 concentration, was observed for 75 µg/ml dose.

4. Discussion

In this study, we assessed in Nanjing, China how fluctuating atmospheric processes, meteorological conditions, and variations in

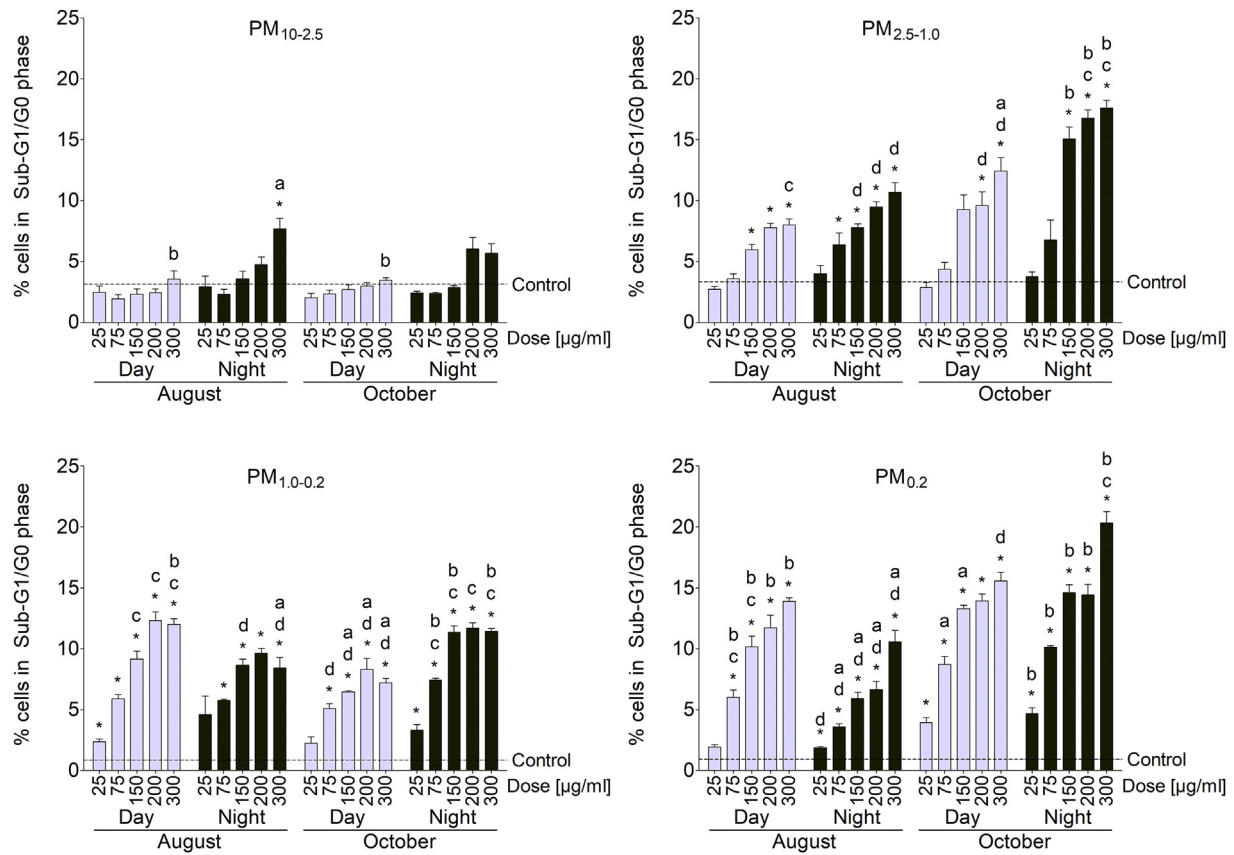


Fig. 9. Cells with severe DNA damage as measured by flow cytometric cell cycle phase analysis on ethanol-fixed and permeabilized PI-stained A549 cells. * denotes significant difference ($p < 0.05$) to control; letters denote significant difference to the same dose of another sample (a August Day, b August Night, c October Day, d October Night). Error bars represent SEM, $n = 4$.

emissions affect the concentration and chemical composition of urban air PM size ranges and their toxicological properties.

During our August campaign, Nanjing hosted the Asian Youth Games (August 16 – August 24, 2013). Thus, the Nanjing government had erected temporary emission control measures in August, including pause of production at key emission enterprises, pause of construction works, and restrictions on road vehicles (Qi et al., 2016). Despite the emission control, industry and traffic were estimated to be the most important sources of trace elements in $\text{PM}_{2.5}$, followed by soil dust, emissions from electroplating and electronics industry, and coal burning. However, during the Asian Youth Games, the contributions of coal burning, industry, and soil dust (attributed to construction) were substantially lower than before the emission control measures. The average $\text{PM}_{2.5}$ concentration of $100.23 \mu\text{g}/\text{m}^3$ reported by Qi et al. during July–August 2013 was significantly higher than the August average $\text{PM}_{2.5}$ concentrations of daytime $35.3 \mu\text{g}/\text{m}^3$ and nighttime $38.4 \mu\text{g}/\text{m}^3$ in the present study. This difference likely highlights the effects of local emissions near the different sampling locations. Indeed, most of the trace element concentrations in the current $\text{PM}_{2.5}$ samples corresponded well with their observations.

Our data show that the air masses in Nanjing during the August sampling campaign were mostly originated in the Northern and Northeastern China, Yellow Sea, Southern China, and East China Sea (2.2, Fig. 2, Sectors 1–3). These sectors encompass vast sea areas, a source for sea spray particles, and contain heavy marine traffic, especially in the Yellow Sea, near Shanghai and coastal waters in general, which produces emissions from fuel oil combustion, such as SO_2 , NO_x and PAHs, contributing significantly to the total PM mixture. The marine aerosols from East China Sea and Southern China cross continental areas before arriving in Nanjing, most notably the heavily polluted mid-YRD region in the East, and the southern megacities, such as the Guangzhou-Shenzhen-Hong Kong region. During the October campaign, the intense fire

activity in the Northeastern China is a likely source of long-distance transported biomass combustion emissions, whereas fire activity near the Eastern China coast and YRD region was much lower than in August (2.1, Fig. 1). The fire map data emphasize the influence of biomass combustion in Northern and Northeastern China in October, whereas the regional biomass combustion emissions in the YRD region were prominent in August. Moreover, during both campaigns there was significant fire activity in the neighboring regions around Nanjing, indicating contributions of local and nearby regional emissions.

In both August and October, the higher PM concentrations during the nighttime compared to daytime are largely affected by the decreased mixing layer depth and calm weather conditions during the night, but they can be influenced by local emission sources as well. The measured masses of size-segregated PM fractions showed that $\text{PM}_{2.5}$, the fraction mainly originated from anthropogenic high-temperature processes, contributed to 43.6–53.8% of total PM_{10} mass during the sampling campaigns. This is in accordance with the results reported by Chen et al. showing annual mean $\text{PM}_{2.1}/\text{PM}_{10}$ ratio of 0.45 ± 0.09 in 2013, and monthly mean ratio of 0.50 ± 0.09 in August 2013 in Nanjing (Chen et al., 2017c). The calculated mass concentrations from the HVCI samples and the measured PM_{10} and $\text{PM}_{2.5}$ mass concentrations from the TEOM measurements showed comparable results.

The atmospheric conditions have large effects on the formation and phase partitioning of secondary aerosols and on the contributions of local and regional transported emissions. Under heavy pollution periods, high relative humidity has been reported to increase the formation of secondary aerosol particles by humidity-related processes, such as heterogeneous reactions in the liquid-phase and condensational particle growth, enhancing the contribution of local emissions. On the other hand, low RH conditions allow for larger contributions of regionally transported emissions in the particle mixture (Tang et al., 2016). The gaseous air pollutants indicate higher anthropogenic emissions in

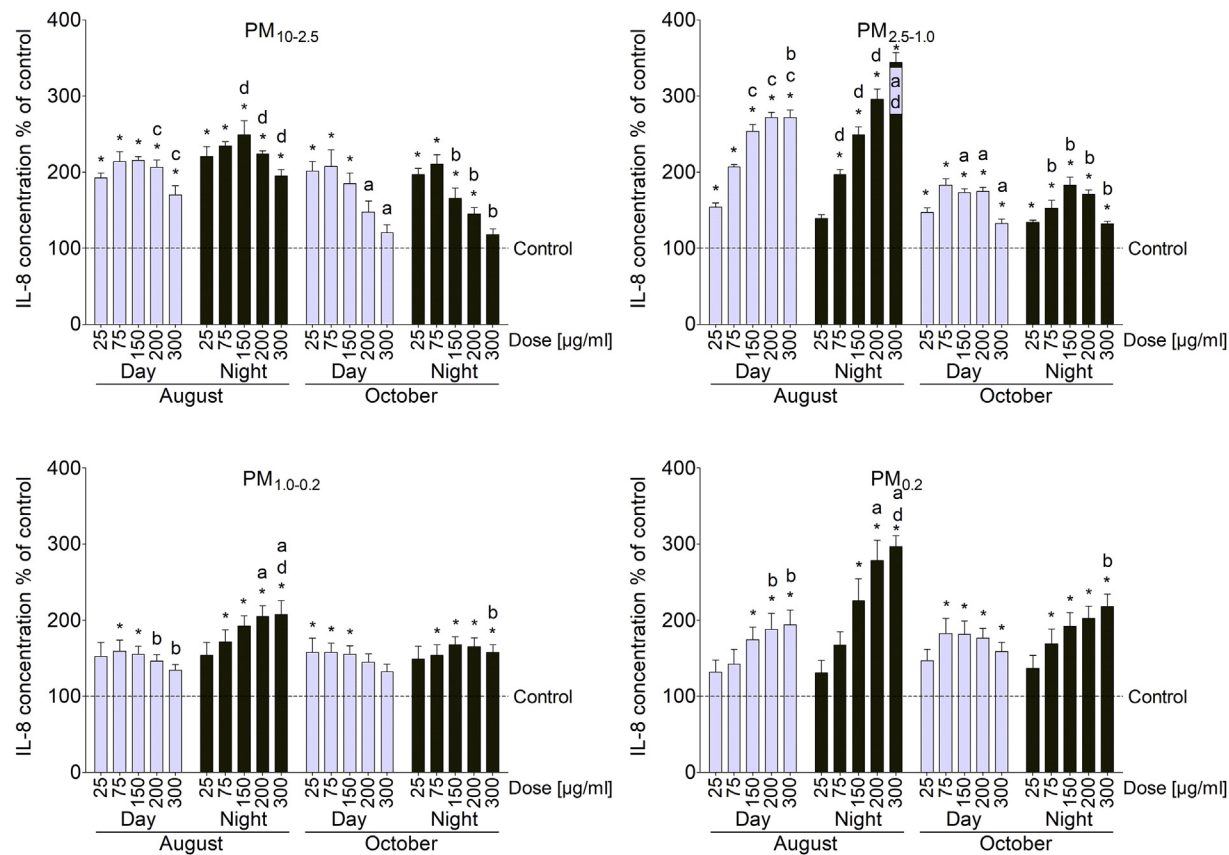


Fig. 10. Secretion of the proinflammatory chemokine IL-8/CXCL8 was measured by ELISA assay from cell culture media collected after the exposure. * denotes significant ($p < 0.05$) difference to control, letters denote significant difference to the same dose of another sample (a August Day, b August Night, c October Day, d October Night). Error bars represent SEM, $n = 4$.

October compared to August. The long-range transport aerosols, which had encountered rainfall much more recently in August than in October, contained assumably less long-range transported PM in August than in October due to particle wet deposition, which reportedly affects especially PM_{10-2.5} (Guo et al., 2016). However, the air mass during the October campaign had spent over twice the time above mixing layer compared to that seen during August, augmenting the regional and local emission contributions. Moreover, the longer time spent in the mixing layer can lead to increased pollutant concentrations and influence of long-range transport in the air parcel in August.

The higher O₃ levels during August were likely affected by the higher temperature and solar irradiance compared to October, which facilitate its formation from precursor aerosols, such as NO_x and volatile organic compounds (VOCs) (Sillman, 1995). Given the relatively similar solar irradiance values during August and October days, and the higher NO_x concentrations in October, the temperature appears to have a large contribution to O₃ formation in August. High tropospheric O₃ concentration is an important contributor to smog formation and is a challenging air quality problem in the densely populated, developed regions in China (Li et al., 2017). On the other hand, the high temperatures in August may lead to reduced partitioning of NH₃ to particle phase, thus yielding elevated gaseous NH₃ levels in August despite the high RH. Wang et al. have reported a linear correlation between gaseous NH₃ concentration and temperature; additionally, they observed a negative correlation between gaseous NH₃ and particulate-phase ammonium (Wang et al., 2015). In contrast, the observed lower gaseous NH₃ concentration in October and the higher NO₃⁻ contents of our PM_{2.5} samples compared to August could be affected by the partitioning of ammonium nitrate to the particle phase at low temperature and high RH conditions (Squizzato et al., 2013).

NO, NO₂, and NH₃ average concentrations exhibited drastic differences between August and October; the significantly elevated levels of NO and NO₂ during October nights indicate extensive fossil fuel combustion, whereas the sharp increase of NH₃ level during daytime August suggests increased agricultural emissions. As reported by Kang et al., the majority of NH₃ emissions in China are from livestock waste and synthetic fertilizers (Kang et al., 2016). However, NH₃ is also attributable to industrial and engine exhaust emissions (Wang et al., 2015). Yet, due to the emission control measures in August, the contribution of local industry and traffic emissions is assumably lower in comparison with October.

Utilizing the experimentally identified diagnostic ratios of specific PAH components proposed by Fu et al., the PAH ratios in the current PM samples generally imply a greater contribution of coal and biomass combustion compared to diesel and gasoline combustion with some temporal variations (Fu et al., 2010). In all PM size ranges and the total PM₁₀, the significantly higher ratio of benzo[b]fluoranthene/fluorene in the night samples compared to day, and in the October samples compared to August, indicates substantially elevated contributions of biomass and coal combustion at night and in October. The fluctuations in the PM₁₀ ratio of dibenzo[a,h]anthracene/fluorene imply diesel and gasoline combustion-dominated emissions during daytime, coal and biomass combustion-dominated emissions at night, and a moderately higher contribution of coal and biomass combustion in October compared to August. The ratio of fluoranthene/(fluoranthene + pyrene) in PM₁₀ also indicates higher contribution of coal and biomass combustion in comparison with fuel and oil combustion (Yunker et al., 2002). The substantially higher ratios of benzo[a]pyrene/benzo[e]pyrene and benzo[a]anthracene/chrysene in the October Night sample when compared to all the other samples can indicate a significantly

larger contribution of fresh emissions and reduced atmospheric aging (Zhang et al., 2017). Picene has been identified as a tracer of coal combustion (Oros and Simoneit, 2000; Zhang et al., 2008), and displayed generally higher concentrations in the night samples compared to day but little variation between August and October, suggesting relatively stable coal combustion in August and October with higher combustion activity at night. A similar day-night pattern was also observed for retene, a tracer of wood combustion (Simoneit et al., 2000), but the difference between August and October was drastic. The retene level in October total PM₁₀ was less than half of August, indicating higher wood combustion activity in August. However, in the absence of specific emission profiles of the local and regional emission sources, the PAH ratios should be considered rather suggestive of the predominant sources. Especially the high amounts of benzo[b]fluoranthene in virtually all our samples can cause exaggerations when estimating the combined contributions of coal and biomass combustion compared to diesel and gasoline combustion.

The observed OPAH size distributions are drastically different when compared to traffic and suburban OPAHs seen in Paris (Ringuet et al., 2012); in our samples the OPAH levels in the PM_{0.2} fraction were extremely low and their concentrations increased drastically in the PM_{1.0–0.2} and PM_{2.5–1.0} fractions. In contrast, Ringuet et al. have reported high traffic and suburban OPAH levels in PM_{0.2} fraction, and decreased concentrations with increasing particle size (Ringuet et al., 2012). However, physical processes in the HVCI during sample collection can influence the observed size-distribution of semi-volatile PAH compounds; for example, desorption from the lower stages induced by low pressure can lead to decreases in observed PAH levels in the smaller size ranges (Di Filippo et al., 2010; Zhang and McMurry, 1991).

Overall, the PAH diagnostic ratios indicate increased contributions of coal and biomass combustion in October and at night, and generally larger contributions of solid fuel combustion in comparison with traffic-related combustion. The role of coal combustion appears to be higher in October than in August. The August Day and Night PM₁₀ diagnostic ratios indicate these two samples had undergone the most extensive atmospheric aging, with only slightly less observed aging for the October Day sample. In contrast, the October Night PM₁₀ displayed drastically larger contribution of fresh PAH emissions. In our previous study of Nanjing urban air PM collected in May 2013 at the same sampling site as in the current study, we reported that sulfated multicomponent particles, as well as soot and other carbonaceous particles were the most common particles in the urban aerosol (Jalava et al., 2015). In that study, the most typical components were C, oxide, K, and S, but trace metals such as Al, Fe, Cu, and Zn were common as well. These findings are mostly in line with the current study. While several metals, like Mg, Si, Na, Pb, and Fe, were associated with the sulfur-rich particles, some particles contained primarily organics (Jalava et al., 2015). These findings demonstrate the complex nature of the composition, sources, and atmospheric transformations of the PM in Nanjing.

4.1. PM_{0.2}

It is well established that urban PM_{0.2} consists primarily of primary local emission particles originated from high-temperature processes in combustion, industry, and traffic. These particles have a short atmospheric lifetime up to several hours, due to particle growth via condensation and coagulation, and their deposition onto surfaces.

In the present study, the chemical characteristics of PM_{0.2} samples showed relatively high PAH content, very low metal and high SO₄²⁻ content, and elevated levels of As, Cd and Cu. Incomplete combustion and pyrolysis of fossil fuels and biomass are the most important sources of atmospheric PAHs (Ravindra et al., 2008), whereas SO₄²⁻ is indicative of fuel combustion and industrial emissions (Reiss et al., 2007). As is an indicator of coal combustion, whereas Cd and Cu are typically prominent in industrial and biomass combustion emissions. Elevated Cu levels have been reported in smelter and power plant emissions in

Nanjing (Chen et al., 2017b). The large fraction of genotoxic PAHs in the samples indicates the high potential for toxicity, as reviewed by Dat and Chang (2017); Kim et al. (2013). Altogether, the chemical profile of the studied samples suggests large contributions from fossil fuel and biomass combustion, and industrial processes. Moreover, detected high PAH content in the October samples implies the increase of combustion processes in the autumn.

Daytime and nighttime samples from the same sampling periods showed substantial variation in composition. The night samples indicated a higher occurrence of fossil fuel and biomass combustion compared to day, likely due to domestic heating. The levels of wood and coal combustion tracer PAHs retene and picene (Oros and Simoneit, 2000; Simoneit et al., 2000; Zhang et al., 2008) were higher in the night samples compared to corresponding day samples suggesting that these activities occurred mostly during the dark hours. The total and genotoxic PAH concentrations were clearly higher in the October samples compared to August and in the night samples compared to day, demonstrating the more extensive combustion activity in October and at night. The atmospheric photochemical reactions and the subsequent chemical degradation of PAHs during the daytime can lead to decreased PAH concentrations, whereas low temperature and mixing layer height, and high RH can act to elevate the PM and PAH concentrations at night. Moreover, the large proportion of calm weather seen in October and especially at night facilitates the accumulation of airborne pollutants. However, given the short atmospheric lifetime of PM_{0.2}, the chemical degradation of PAHs in this size range is likely a less important factor in comparison with the size fractions with longer atmospheric lifetimes, such as PM_{1.0–0.2} and PM_{2.5–1.0}. Regardless, the August Night sample contained the most picene and retene in this size range with over twice the concentration of retene compared to the October Night sample, suggesting increased contributions of local coal and especially wood combustion in August. However, this is in contrast with the total PAH concentrations in the samples and the drastically higher K concentrations in the October samples compared to August samples.

Potassium has been related to a number of sources including biomass and garbage combustion (Hu et al., 2013; Li et al., 2010; Yang et al., 2017). Chen et al. reported enriched K and Mn in local straw burning emissions in Nanjing and Wuxi, and identified straw burning as one of the major source of particulate K; K and Pb were also observed for garbage incineration emissions, possibly due to kitchen and household waste (Chen et al., 2017b). Contrasting with the PM size-distribution of K from biomass combustion reported by Chen et al., the samples in the current study show higher proportions of K in the smaller size ranges. Overall, biomass combustion is likely an important source of K in the smaller, high-temperature process-derived particles in the current study. The temporal and regional variations in biomass burning in China are large. In general, the biomass contribution is lower in winter when coal combustion-based heating systems dominate, but increases in summer and autumn during harvesting periods, as reviewed in (Chen et al., 2017a). The slightly larger contribution of southerly winds during October nights and their relative absence during October days add another source of variation into the composition of the PM mixture, increasing the influence of local emissions from south of the sampling site.

Previously, Zn has been associated with emissions from industrial and motor vehicles, as well as incinerators (Hu et al., 2013; Liu et al., 2014). High temperature-derived particles rich in Fe and containing Mn or Zn have also been linked to metallurgic emissions (Hleis et al., 2013). Moreover, August samples contained slightly more SO₄²⁻ than October samples, with elevated amount in the day samples. This points to enhanced photochemical transformations of sulfur oxides in sunlight; in addition, the elevated concentration in the Day samples could be due to traffic or ship emissions on the nearby Yangtze River in the North, supported by the prevailing wind directions and air mass trajectories from sectors 1 and 5. In contrast, October samples contained substantially more NO₃⁻ and the levels were higher in night samples than

daytime samples. This may indicate increased coal combustion or traffic emissions in October and during the dark hours, or increased NO_x oxidation via nitrate radical-dependent reactions when the solar irradiance is low (Stockwell et al., 2003). However, the secondary inorganic aerosols have little evidence of causing toxicity (Grahame and Schlesinger, 2005; Reiss et al., 2007; Schlesinger and Cassee, 2003).

4.1.1. Toxicological characteristics of PM_{0.2}

PM_{0.2} particles caused substantial effects on the cell cycle, metabolic activity, and inflammatory response of A549 cells. The October samples elicited larger proportion of cells in the Sub-G1/G0 population than August samples, indicating extensive DNA damage or degradation, such as that caused by apoptosis. This is likely influenced by the much higher total and genotoxic PAH concentrations in the October samples. Environmental PAHs have been reported to cause DNA damage and influence the cell cycle (Bai et al., 2017), but there is also evidence of non-additive and inhibitory effects of complex PAH mixtures on genotoxicity and DNA damage (Genies et al., 2016; Líbalová et al., 2014). Structural characteristics of PAHs and their derivatives can cause large differences in cellular responses, as demonstrated by the strong cytotoxic effects of redox-cycling ortho-quinoid PAHs when compared to redox-inactive para-quinoid PAHs (Motoyama et al., 2009).

The current samples represent a complex mixture of PAHs and inorganic species with a significant portion of unidentified chemical species, all of which can interact to create variability in the cellular responses. The Day samples in both campaigns showed similar increases of Sub-G1/G0 population, but the difference between the Night samples of the two sampling campaigns was very large. The similar responses for the two day samples despite the large differences in the observed chemical compositions suggests divergent pathways leading to the observed effects, while the interaction of the identified and the unanalyzed components may influence these results as well. In addition to the increased Sub-G1/G0 population, all samples caused decreased G1/G0 populations, and the highest doses of the Night samples greatly diminished S/G2/M population. These findings suggest cell death with increasingly degraded DNA and largely intact cellular membranes, such as apoptosis, occurring during all phases of the cell cycle. This is supported by the discrepancy of greatly decreased CMA and only slightly increased permeability of the cellular membranes, which indicate that necrotic cell death is not responsible for the observed cytotoxicity. Moreover, the lack of observed dose-dependent cell cycle blocks and the large amount of cells in Sub-G1/G0 population suggest that the DNA repair capacity is exceeded, likely resulting in apoptosis.

Most metal constituents, SO₄²⁻, NO₃⁻, PAH compounds, and genotoxic PAHs were strongly associated with the observed cell cycle effects. For example, K, the most abundant metallic species in our samples, and benzo[a]pyrene displayed strong positive correlations for the increased Sub-G1/G0 population (ρ 0.904 for K; ρ 0.887 for benzo[a]pyrene), strong negative correlations with the G1/G0 (ρ -0.627 for K; ρ -0.617 for benzo[a]pyrene), and moderate or strong negative correlations with the S/G2/M populations (ρ -0.621 for K; ρ -0.573 for benzo[a]pyrene). As discussed above, K is likely from combustion processes, but it may act as a surrogate for more toxic combustion-derived components; the same applies for the secondary inorganic ions SO₄²⁻ and NO₃⁻. Previously, Könczöl et al. have studied toxicological effects of several different metal particles, such as ZnSO₄, PbSO₄ and magnetite (Fe₃O₄) and reported of cell cycle alterations in the exposed A549 cells. In their studies, ZnSO₄ induced arrest in G2 phase, whereas PbSO₄ increased the Sub-G1/G0 population paired with an increased genotoxic response (Könczöl et al., 2012). In the current samples, Pb and Zn displayed strong positive correlations with the increased Sub-G1/G0 population and moderate negative correlations with the G1/G0 population. Magnetite has been observed to cause increased Sub-G1/G0 and decreased G1/G0 populations independently of particle size; however, no indication for activation of the proapoptotic pathway was found (Könczöl et al., 2013). Several other metals in our samples displayed

strong correlations with the increased Sub-G1/G0 population, but their correlations to the G1/G0 and S/G2/M population sizes were weaker or insignificant.

Although the genotoxic responses for this size range were rather low, the increased Sub-G1/G0 population and genotoxic response measured by SCGE showed a moderate positive correlation (ρ 0.597). The genotoxic response could contribute to the observed extensive DNA degradation in the cells, possibly through DNA damage-induced apoptosis. The proinflammatory response also displayed a moderate positive correlation with the Sub-G1/G0 response (ρ 0.537), suggesting the interaction of proinflammatory mechanisms and the degradation of cellular DNA. The loss of cell membrane integrity showed no significant correlations with the cell cycle effects, implying the effects were unrelated to cell membrane disruption caused by, for example, necrosis. Although the observed oxidative stress responses after 24 h exposure for PM_{0.2} in the current study were at the base line or slightly below it, significant oxidative stress may have occurred earlier during the exposure, as observed for PM_{2.5} by Deng et al. (2013). Thus, it is possible that the oxidant producing chemical species have depleted their reactivity at the 24 h time point, and have caused their toxic effects earlier.

Genotoxic PAHs displayed a moderate association (ρ 0.506) with the genotoxic response, whereas total PAH and OPAH, and genotoxic PAH concentrations were both very strongly associated with the observed cell cycle effects. PM_{2.5} has been reported to induce apoptosis of A549 cells via mitochondrial production of ROS (Soberanes et al., 2009). Additionally, water-soluble PM_{2.5} extracts have been linked to oxidative stress, disturbances in metabolism and signal transduction, imbalanced protein synthesis and degradation, as well as disorganization of cytoskeleton in A549 cells; induction of apoptosis has also been suggested as a key toxicological event (Huang et al., 2014). PAH-derived diol epoxides, redox cycling quinones, and radical cations formed via metabolic transformations of PAHs can result in bulky DNA adducts and oxidative DNA damage, and modulate DNA repair mechanisms, cell cycle progression, and cell fate (Mattsson et al., 2009; Penning et al., 1999; Roos et al., 2016). Overall, several pathways can lead to the observed effects on cellular DNA and cell cycle, and the particle composition may influence the selection and extent of activation of these pathways.

The August samples showed higher ability to hinder cellular metabolism of A549 cells in comparison with the October samples. Most metal constituents and SO₄²⁻ were strongly associated with the reduced CMA and decreased cell membrane integrity. In contrast, only a handful of analyzed PAHs showed strong correlations with CMA response and total PAH level showed no significant association with decreased cell membrane integrity. PAH, metal, and transition metal concentrations have all been associated with cytotoxicity of PM in several studies, and the cytotoxic effects tend to be greater in the smaller PM size ranges (de Kok et al., 2006), while the secondary ions such as SO₄²⁻ and NO₃⁻ are generally considered surrogates and not responsible for the toxicological effects (Grahame and Schlesinger, 2005; Reiss et al., 2007; Schlesinger and Cassee, 2003; Schlesinger, 2007). However, sulfuric acid can cause the dissolution of metals in the particulate phase, leading to increased levels of particulate soluble metals; in the case of redox-active transition metals, this can lead to elevated oxidative potential of the particles (Fang et al., 2017).

The strongest correlations for reduced CMA were observed for As, Cr, Cu, Ni, Pb, and Zn. Perrone et al. have reported similar findings of reduced CMA in A549 cells associated with As, Zn, Cu, Cr and SO₄²⁻ present in PM_{1.0} and PM_{2.5} (Perrone et al., 2010). Deng et al. have also observed autophagy triggered by PM_{2.5}-induced oxidative stress in A549 cells, providing another pathway potentially resulting in cell death (Deng et al., 2013). Indeed, the oxidative stress response showed a strong negative association with the decreased CMA (ρ -0.755) and a very strong negative correlation with cell membrane integrity (ρ -0.755), but no correlations with other toxicological endpoints, suggesting a direct cytotoxic pathway linked to oxidative stress. Toxic metals such as Cr, Cu, Pb, and Zn, as well as SO₄²⁻ displayed strong positive correlations with

the oxidative stress response, which suggests the metal sulfates were largely responsible for the oxidative response. In contrast, the overall PAH and OPAH levels, benzo[a]pyrene, and benzo[k]fluoranthene showed no correlations with oxidative stress. Interestingly, picene (ρ 0.900) and retene (ρ 0.846) displayed very strong correlations with the oxidative stress, implying that some PAHs may contribute to the oxidative stress response. The PM_{0.2}-induced inflammatory response mediated by IL-8/CXCL8 showed distinct variations between August and October with generally lower responses for October samples, and the greatest response elicited by the August Night sample was significantly higher than that of August Day and October Night. However, virtually all components present in the PM_{0.2} samples showed strong or very strong positive correlations with the inflammatory response.

In summary, these results indicate that the present PM_{0.2} samples caused cell cycle perturbations and cellular inflammatory reactions in A549 cells. Furthermore, they suggest that the reduced CMA is more closely linked to the inflammatory response than the cell cycle effects, and while the October samples caused more severe cell cycle alterations, the August samples were ultimately more cytotoxic. Metal components were the most negatively associated with cell viability while showing strong associations with oxidative stress, and some of them showed strong associations with the cell cycle responses. In contrast, PAHs and OPAHs were generally strongly associated with the cell cycle effects, and virtually all components appeared responsible for the inflammatory response.

4.2. PM_{1.0–0.2}

A substantial portion of the PM_{1.0–0.2} fraction originates from primary emissions that undergo chemical and physical transformations in both gaseous and particulate phases, such as condensation of vapors on primary emission particles and agglomeration. These grown particles are mostly covering the accumulation mode in the atmosphere. Other particle sources in this fraction are fresh emissions from incomplete combustion and new particle formation caused by photochemical reactions of volatile organic compounds and nitrogen oxides. Resulting from the very long atmospheric residence time ranging from days to weeks as well as low mass, the particles in this fraction are readily transported by winds to distant locations and contribute to smog episodes.

In the present study, SO₄²⁻ and NO₃⁻ dominated the chemical composition, indicating the large contribution of the aged, long-range transported secondary inorganic aerosols (Itahashi et al., 2016; Ying et al., 2014) with a relatively large fraction of PAHs and low proportion of metals. The increased amount of SO₄²⁻ in the day samples can be attributed to enhanced photochemical formation of particulate sulfates. On the other hand, the low NO₃⁻ levels in the August samples and higher levels in the night samples compared to day demonstrate the role of photolysis and nightly accumulation of nitrate radical (NO₃) required for the heterogeneous reactions between N₂O₅ and particle-bound liquid water to form nitrate particles (Stockwell et al., 2003). The higher PAH levels in the October samples compared to August, and in the night samples compared to day indicate more combustion activity and decreased atmospheric transformations in October and at night. Yet, the low retene and picene levels in this size range suggest a significant contribution of aged combustion emissions in which these PAHs have been lost due to atmospheric chemical reactions. In these samples 1,8-naphthalic acid anhydride and 9,10-anthracenedione were the two most abundant OPAHs comprising a substantial proportion of total PAHs and OPAHs. In general, OPAHs can be directly emitted from combustion processes or emerge as secondary organic aerosols formed via atmospheric transformations induced by UV radiation and reactions with atmospheric oxidants (Walgraeve et al., 2010). However, given their extremely low concentrations in the PM_{0.2} samples, they are possibly more associated with aged emission particles than fresh combustion particles in our PM_{1.0–0.2} samples. The notable level of genotoxic PAHs in the samples indicates the toxic potential still present in the

samples, whereas their lower levels in the day samples compared to night implies the loss of these chemical components due to atmospheric transformations. The reduced mixing volume at night also contributes to the high nighttime PAH levels. In the relatively small observed metal fraction, notable contributions are seen for Al and Ca, likely originated in various industries such as metallurgic, cement, and ceramic industries, indicators of biomass combustion K and coal combustion As, and Zn, Cr, Cu, Mn, and Pb which can be from a wide variety of sources including construction, traffic and industrial emissions (Chen et al., 2017b; Chow et al., 2004). Additionally, Fe has been observed to be an important element in coal combustion-derived PM (Ruan et al., 2018). K clearly dominates the metal composition in the October samples, with higher level in the night sample compared to day, suggesting increased biomass burning and waste incineration (Chen et al., 2017b). The slightly increased Zn concentration in the October samples compared to August could indicate higher traffic volume; this is in agreement with the local traffic restrictions in August, but long-range transport can also affect the Zn levels in this size range.

4.2.1. Toxicological characteristics of PM_{1.0–0.2}

The cellular responses for our PM_{1.0–0.2} samples were generally quite low. The most notable toxicological effects caused by our PM_{1.0–0.2} samples were the cell cycle effects and the genotoxic response. Additionally, we observed higher responses of CMA reduction and oxidative stress for the August samples compared to October, and higher inflammatory response for the August Night sample.

The August Day and October Night samples produced similar proportions of cells in the Sub-G1/G0 cell cycle phase, whereas August Night and October showed lower responses. In addition, the August Day and October Night samples caused the greatest decreases of G1/G0 and S/G2/M phase populations. These findings are largely similar to those observed for our PM_{0.2} samples, indicating DNA degradation throughout the cell cycle, likely via apoptosis. Virtually all PAHs and metals, and SO₄²⁻ were strongly associated with the observed effects on Sub-G1/G0 and S + G2/M populations, but only As and retene displayed significant, although only moderate, negative correlations (As ρ -0.469, retene ρ -0.503) with the G1/G0 population size. Additionally, As, Cd, Cr, Ni, Pb, Zn, SO₄²⁻, total PAHs and OPAHs, and OPAHs displayed strong or very strong positive correlations with the oxidative stress response, which was again strongly correlated with the cell cycle response (ρ 0.707 for Sub-G1/G0 population and ρ -0.682 for S + G2/M population). This implies the relation between oxidative damage and the observed cell cycle effects. Several components showed their highest concentrations in the October Night sample in this size range, whereas most of these were seen at their lowest level in the August Day sample. Atmospheric aging of PM has been shown to enhance the toxicity of PM due to increased oxidative potential (Verma et al., 2009). The higher rate of photochemical reactions of PAHs in the August Day sample could possibly lead to increased toxicity via the atmospheric activation of PAHs into chemical species able to induce oxidative damage, such as redox-active quinones and radicals (Fu et al., 2012).

All samples except August Day elicited significant genotoxic responses, but the effect magnitude remained quite low. The August Day sample contained significantly less genotoxic PAHs than the other samples, which likely explains the insignificant response. The genotoxic PAHs and benzo[a]pyrene were moderately associated with the genotoxic response (ρ 0.512 for genotoxic PAHs and ρ 0.512 for benzo[a]pyrene), whereas benzo[k]fluoranthene displayed a very strong correlation (ρ 0.806). In addition to PAHs, Al (ρ 0.706), Cl⁻ (ρ 0.732) and NO₃⁻ (ρ 0.791) displayed strong positive correlations with genotoxicity while K (ρ 0.565) and Mn (ρ 0.571) exhibited moderate positive correlations. Previously, Mn in PM_{1.0} has been associated with cytotoxicity and DNA damage (Perrone et al., 2010). These components displayed higher concentrations in the October samples compared to August suggesting their role in the elevated genotoxic response for the October samples. The high correlation coefficients of Cl⁻ (ρ 0.732) and NO₃⁻ (ρ

0,791) with the genotoxic response suggest the large contribution of secondary emission particles to the genotoxic responses, but their low correlations with the other toxicological responses imply they are likely surrogates for the toxic components, such as transition metals associated with them. Previously, Perrone et al. have reported of oxidative stress and DNA damage caused by combustion-derived PM_{2.5} and PM_{1.0} (Perrone et al., 2013).

Most metals and total PAHs and OPAHs displayed strong or very strong negative associations with both CMA and cell membrane integrity; most of these also displayed strong associations with the oxidative stress response suggesting the detrimental effects on cellular metabolism and viability are linked to oxidative stress. Moreover, the increased Sub-G1/G0 population displayed a very strong negative correlation with CMA ($\rho = -0.839$), suggesting the cytotoxic effects of our PM_{1.0–0.2} samples on A549 cells were greatly influenced by cell cycle disruption, likely via induction of apoptosis.

Overall, our results suggest that the toxicological responses elicited by PM_{1.0–0.2} were in line with those observed for PM_{0.2}, but at lower magnitude. The high proportion of typically secondary aerosol components suggests the prominent role of atmospheric aging and long-range transport in this size range. The atmospheric aging of aerosols and the dilution of fresh emissions with secondary aerosols likely contribute to the observed decreased toxicological effects.

4.3. PM_{2.5–1.0}

This size range consists primarily of older emission particles with some influence from fresh emissions, as well as the smallest coarse mode particles, such as suspended crustal and biogenic particles, and particles formed by anthropogenic mechanical processes, e.g. brake wear. A considerable portion of this size range can be from distant sources relocated via long-range transport. The aged particles can contain a diverse assortment of chemical components, a cause for substantial composition-dependent variations in toxicological responses (Jalava et al., 2016). Given the prevalence of long-range transport particles in this size range, the meteorological conditions and atmospheric processes have a profound influence on the composition.

Our data show that the composition of this size range is dominated by SO₄²⁻ and NO₃⁻, indicating a significant proportion of aged, long-range transported particles. Moreover, the increased proportion of NO₃⁻ in comparison with SO₄²⁻ suggests larger contributions of aged fuel combustion emissions than in the smaller PM fractions. The relatively high levels of Al, Ca, Fe, and Mg compared to the smaller size ranges indicate the increased role of crustal material. However, Ca and Fe-rich particles in the fine mode can be linked to metallurgical emissions, since Ca-based compounds are used as raw materials in the sintering process (Landkoc et al., 2017; Machemer, 2004). In the YRD-region, Chen et al. have associated Ca with emissions from cement and ceramic industry, and coal-fired power plants (Chen et al., 2017b). Moreover, Al in Beijing PM_{2.5} has been linked with metal processing and construction emissions (Liu et al., 2014), and Fe can be enriched in coal combustion emissions (Ruan et al., 2018). On the other hand, the relatively low levels, compared to the smaller size ranges, of As (coal combustion), Cu (industry, traffic, and brake wear), K (biomass and waste incineration) and Pb (smelting, industry) suggest a smaller role of these emission sources in this size range (Chen et al., 2017b). However, their concentrations were generally higher in the October samples in comparison with August, indicating the influence of emission control measures in August, the northerly air masses in October, and the atmospheric processes. These results indicate the pronounced role of both fossil and biomass combustion emissions in October and at night. This is supported by the increased total and genotoxic PAH levels in the October samples compared to August, and in the night samples compared to day, but the PAH concentrations are also influenced by the photochemical transformations. The Zn concentration in particles,

which was higher in October than in August, indicates important contributions from industry and traffic emissions (Liu et al., 2014).

The very high total PAH + OPAH concentrations suggest substantial contribution of combustion processes in this size range. In general, the observed concentrations of unsubstituted and alkylated PAHs, and genotoxic PAHs were at similar levels compared to PM_{1.0–0.2} and PM_{0.2}. However, the proportion of OPAHs out of total PAHs and OPAHs was the greatest in this size range and distinctly elevated in the August compared to October, and day in comparison to night. This implies the strong influence of atmospheric photochemical reactions, which can decrease the amount of parent PAHs, and yield increased concentrations of secondary PAHs, such as certain OPAHs. However, as discussed in conjunction with PM_{1.0–0.2}, OPAHs can be partly primary organic aerosols, but distinguishing primary and secondary organic aerosols is out of scope of this study. In contrast to PM_{0.2} and PM_{1.0–0.2} where the unsubstituted, alkylated, and genotoxic PAH levels were significantly greater in the October samples, in PM_{2.5–1.0} samples this difference is diminished with October samples containing only slightly more PAHs in comparison to August samples. Indeed, the genotoxic PAH levels in the August PM_{2.5–1.0} samples were clearly higher than those seen in August PM_{0.2} samples, making PM_{2.5–1.0} the size range with the greatest amount of genotoxic PAHs in August. This could be due to relatively fresh combustion emissions, or very high atmospheric concentrations of transported PAH-containing aerosols, which can result in such high PAH levels despite the greater photochemical activity in August and during the daytime. The foremost OPAH species were 1,8-naphthalic acid anhydride, 9H-fluoren-9-one, and 9,10-anthracenedione. These are rather common OPAHs in urban air originated from a variety of sources; 1,8-naphthalic anhydride can also be found as secondary organic aerosol (Ringuet et al., 2012; Wei et al., 2012). In addition, xanthone, typically observed in the atmosphere near sources of wood combustion emissions (Orasche et al., 2012; Orasche et al., 2013), was detected only in the October Night sample. This suggests a local source producing rather large particles from poor combustion, which could contribute to the high PAH concentrations. However, this size partitioning for xanthone is rather unusual, and could be influenced by the sample collection.

4.3.1. Toxicological characteristics of PM_{2.5–1.0}

The greatest toxicological responses caused by our PM_{2.5–1.0} samples were the reduction of CMA, the cell cycle effects, and the high inflammatory response. CMA reduction was strongly associated with virtually all chemical components except K, SO₄²⁻, and fluorine. The difference of CMA reduction elicited by the August and October samples were small, but significant between the day samples; in general, August samples were more detrimental for A549 metabolism than October samples. The August samples contained slightly lower amounts of metals compared to October, whereas PAHs and OPAHs were observed in higher concentrations in the August samples; thus, PAHs and OPAHs likely influence the increased CMA reduction. Indeed, total PAHs and OPAHs ($\rho = -0.892$) and OPAHs ($\rho = -0.940$) displayed the highest negative correlations with CMA after Cu ($\rho = -0.961$), Cr ($\rho = -0.940$), and Ni ($\rho = -0.904$), which were observed at low concentrations. Perrone et al. have previously reported of greater reduction of CMA in A549 cells caused by spring and summer PM from Milan in comparison with fall and winter PM (Perrone et al., 2013). CMA displayed strong negative associations with very similar correlation coefficients for oxidative stress, inflammation and the increased Sub-G1/G0 population size, suggesting that these three pathways contributed to the reduction of CMA. However, these three pathways showed no associations between each other, suggesting that they elicit their responses with little to no interaction with each other.

The cell cycle responses of increased proportion of cells in the Sub-G1/G0 phase and reduced proportions of G1/G0 and S/G2/M phase were higher for the October samples compared to August, higher for the Night samples compared to Day, and drastically pronounced for

the October Night sample. These results are quite similar to those observed for our PM_{0.2} samples, suggesting the role of similar, possibly local, emission sources contributing to the cell cycle effects. Virtually all components except As, Na, and SO₄²⁻ showed strong or very strong correlations with the increased Sub-G1/G0 population size and negative correlations with the S + G2/M population size. Interestingly, OPAHs displayed lower, although strong, correlations with these population sizes than other PAHs. In contrast, OPAHs displayed a strong positive correlation (ρ 0.632) with the genotoxic response along with As, Cu, and retene, whereas other PAHs showed no correlations. In addition, these components were strongly associated with the inflammatory response, which in turn had a moderate, yet not significant correlation with the genotoxic response, suggesting a possible interaction of inflammation and DNA damage. The observed cell cycle effects could potentially influence the stunted proinflammatory responses for the October samples, i.e. high doses of the October samples could possibly decrease the production of IL-8/CXCL8 due to cytotoxicity. However, certain components, such as some oxygenated and nitrogenated PAHs, can inhibit the production of IL-8/CXCL8 (Koike et al., 2014), which fits better with the current observations since the October samples elicited lower reduction of CMA in comparison with the August samples. The possibly nearby local emission source implied by the presence of xanthone in the October Night sample could possibly explain the great cell cycle response for this sample.

Furthermore, the very low genotoxic responses elicited by our PM_{2.5-1.0} samples suggest the DNA degradation displayed in cell cycle analysis is likely linked to apoptosis, and not to extensive chemical-induced DNA damage. Previously, oxygenated and nitrogenated PAHs have been observed to contribute substantially to mutagenicity of PM_{2.5} particles in Beijing (Wang et al., 2011), and there is evidence for ROS formation induced by OPAHs in PM_{2.5} (Sklorz et al., 2007). The OPAHs and other PAHs in our PM_{2.5-1.0} samples displayed moderate correlations with the oxidative stress response, whereas strong positive correlations were observed for Al, Ca, Cd, Cr, Mg, Ni, and Pb. Thus, oxidative stress by both metallic and organic components appears a likely cause for the observed cellular effects.

In summary, the current PM_{2.5-1.0} samples caused drastically disturbed cell cycle in the form of increased Sub-G1/G0 population, likely due to apoptosis. Furthermore, the samples caused great reductions of cellular metabolic activity. The August samples produced very high inflammatory responses while the responses for October samples were low and displayed very low IL-8/CXCL8 production for the highest doses. The results suggest that CMA was influenced by the cell cycle effects, inflammatory response, and oxidative stress. However, the finding that the cell cycle, oxidative stress, and inflammatory responses showed no correlations with each other suggests that the different emission sources and the associated changes in chemical composition of PM induce different pathways of toxicity in A549 cells.

4.4. PM_{10-2.5}

Particles of this size range originate from a variety of sources including crustal minerals, sea salt, mechanically generated anthropogenic emissions, such as traffic dust from road wear and tire abrasion, and biogenic material such as pollen and microbial or fungal components. PM_{10-2.5} settling and deposition from the air can be fast in calm weather conditions, but wind-borne particles of this size range are subject to intra- and inter-regional long-range transfer during dust storms. Typical atmospheric residence time for this size range is from hours to days. We found comparably high contents of metals from crustal origin, such as Al, Ca, Mg and Fe, in all PM_{10-2.5} samples and their concentrations were significantly higher in the October than August samples. This indicates an influence of long-range transport of air masses from Northern China in October as well as continued construction work after the August emission control period. Contrarily, Na concentration was drastically higher in the August samples, which was likely influenced by

wind-borne sea spray from the Eastern China Sea. This is supported by the higher Cl⁻ and NO₃⁻ concentrations in the August samples, which indicate larger contributions of secondary inorganic aerosols in comparison with October.

The observed total PAH levels were quite similar between the sampling campaigns, but displayed significant day-night variations with twice the PAH concentration seen in the night samples compared to day, which is attributable to PAHs adsorbed onto the particles, the overall higher PAH concentrations at night, and photochemical transformations during the day. A similar day-night pattern was observed for the genotoxic PAHs as well, but the August samples contained substantially more genotoxic PAHs than the October samples. This is in stark contrast with the smaller size range samples where the October samples contained higher levels of genotoxic PAHs.

Overall, the PAHs and OPAHs showed large variations between August and October. Concentrations of phenanthrene, fluoranthene, pyrene and 9,10-anthracenedione were drastically higher in the August samples compared to October, whereas the October samples contained much higher amounts of OPAHs, namely 9H-fluoren-9-one and xanthone. These findings suggest different source profiles and influences of atmospheric processes between the campaigns. 9,10-anthracenedione has been observed to be an important OPAH in the coarse particle fraction in Parisian air both near traffic and in suburban areas, whereas 9H-fluoren-9-one was found primarily in suburban air (Ringuet et al., 2012). Temperature, relative humidity and wind speed have been observed to influence the size-distribution of PAHs between fine and coarse fractions via mechanisms such as evaporation, condensation, and adsorption; high PAH concentrations in the coarse particle fraction have been attributed to PAHs transferring from fine to coarse particles (Meng et al., 2015; Teixeira et al., 2012). Furthermore, PAHs and halogenated PAHs have been reported to be enriched in the coarse particle fraction in emissions produced by solid waste incinerators, and showed high concentrations near the emission source (Shu et al., 2018). In summary, the PAHs in the present PM_{10-2.5} samples can be from traffic, aged combustion emissions and from poorly controlled local solid fuel combustion, and may have undergone transfer from fine-mode particles into coarse particles.

4.4.1. Toxicological characteristics of PM_{10-2.5}

PM_{10-2.5} samples caused by far the greatest genotoxic and oxidative stress responses in our current data, and an inflammatory response with very high IL-8/CXCL8 concentrations for the lowest doses, which declined with the increasing dose after a threshold. Previously, transition metal-dependent hydroxyl radical formation has been reported to induce DNA damage in A549 cells using the SCGE assay, and the presence of particles further enhanced the genotoxicity (Knaapen et al., 2002). The high oxidative stress response for PM_{10-2.5} showed very strong associations with most metals in our samples, and is likely attributed to high amounts of transition metals; the higher oxidative response for the October samples coincides with higher Al and Fe mass fractions compared to the August samples. However, while the redox-active transition metals have been suggested to be involved in the oxidant activity of PM, no clear causative components have been identified (Künzli et al., 2006). Previously, Janssen et al. have discussed the role of transition metals inducing high oxidative stress responses for PM_{10-2.5}, and reported moderate to high correlations of oxidative potential with PAHs in PM₁₀ and PM_{2.5} (Janssen et al., 2014). However, they did not see significant correlation between oxidative potential and PAHs for PM_{10-2.5}, and suggested that this is likely caused by the relatively low levels of PAHs in the fraction. Oxidative stress displayed a very strong negative correlation with CMA (ρ -0.815, p < 0.01), suggesting the cytotoxicity was influenced by oxidative damage.

The high inflammatory response and oxidative stress for PM_{10-2.5} has been associated with endotoxin and other microbial or fungal components, and with high metal and carbon contents. Of the metal constituents, crustal and other non-exhaust metal elements in this size range

have been associated with the inflammatory response (Jalava et al., 2016; Michael et al., 2013; Soukup and Becker, 2001; Steenhof et al., 2011). The significant differences between the four samples observed on the decreasing parts of the dose-response curves indicate composition-influenced inhibition of IL-8/CXCL8 production. We speculate that the steeper decline of IL-8/CXCL8 concentration induced by the October samples could be due to the higher Ca and/or OPAH concentrations in comparison with the August samples, though several kinds of organic compounds can potentially affect the cytokine release. Koike et al. have reported inhibition of IL-8 production in human bronchial epithelial cells exposed to oxygenated and nitrogenated derivatives of naphthalene, phenanthrene, and pyrene, while the parent PAHs induced no changes (Koike et al., 2014). Additionally, ambient PM has been observed to suppress cytokine levels released by alveolar macrophages by influencing the intracellular retention and secretion, and overall production of cytokines (Sawyer et al., 2009). In addition, disturbance of the cellular Ca-homeostasis could affect the Ca-dependent IL-8/CXCL8 secretion. Furthermore, Michael et al. have observed dose-dependently decreasing IL-8 levels in A549 cells exposed to PM₁₀ (Michael et al., 2013). It has been suggested that cytokine adsorption to particles could affect the observed cytokine release; this is largely related to particle surface area and carbon content (Akhtar et al., 2010). However, this hypothesis fits poorly with the current data regarding the particle surface area, which is relatively small in the coarse particle fraction and usually dominated by the accumulation mode (Seinfeld and Pandis, 2006). Moreover, the presence of serum proteins in the culture medium during the exposure renders extensive nonspecific binding of cytokines onto particles unlikely. The high DNA damage and decreased cellular metabolic activity levels can also contribute to the dose-dependent decrease of IL-8/CXCL8 production, either directly through cytotoxicity or via a damage-response shift of focus from extra-cellular signaling to repair and survival. Yet, since the observed decrease of CMA was relatively modest for this size range and displayed no August/October or day/night variations, the CMA reduction alone is insufficient to explain the observed differences in dose-dependent decrease of IL-8 secretion.

The extremely high genotoxic response paired with no increase of Sub-G1/G0 cell cycle phase population indicates that the genotoxic effects observed by SCGE are transient or do not lead to extensive DNA degradation, or do so in a delayed fashion. A similar pattern of significant oxidative stress and genotoxicity with no cell cycle effects in A549 cells have been observed for CaSO₄ particles, caused by increased ROS production and consequent oxidative DNA damage (Könözöl et al., 2012). In the currently employed alkaline SCGE, observed DNA damage can be caused by DNA strand breaks or alkaline labile sites caused by e.g. alkylations, oxidations or base-less sugar intermediates of base excision repair. Yet, the high oxidative stress response suggests the observed genotoxicity is likely due to oxidative DNA damage, such as formation of 8-hydroxy-2'-deoxyguanosine (8-OHdG) and 8-oxo-7,8-dihydro-2'-deoxyguanosine (8-oxodG) (Valavanidis et al., 2013). Furthermore, the very low response for cell membrane disruption demonstrates that cell membranes of PM_{10-2.5}-exposed cells were mostly intact, which renders necrosis unlikely. Interestingly, PM_{10-2.5} was the size range with the lowest observed genotoxic PAH content, and the concentrations of genotoxic PAHs and OPAHs in the single samples do not correspond to the observed genotoxic responses. However, genotoxic PAHs and OPAHs displayed strong positive correlations with the genotoxic responses, whereas of metals the only significant correlations with the genotoxic response were the moderate positive correlations of Cu and Zn. In contrast, Perrone et al. have reported of predominantly transition metal driven DNA damage in A549 cells, but they discuss the possibility of masked influence of PAHs (Perrone et al., 2010). In this regard, the strong correlations by genotoxic PAHs and OPAHs display the importance of PAHs even if their concentrations are relatively low, such as in the present PM_{10-2.5} samples. Although the correlations of the single metals show little support, the very high metal concentration in the PM_{10-2.5} samples is likely the driving force behind the observed

genotoxicity of PM_{10-2.5}, but PAHs likely contribute as well. Even though the genotoxic response caused by our PM_{10-2.5} samples is likely influenced by the high oxidative stress and inflammatory responses, they show no significant associations and display somewhat contrasting results when comparing the four different samples. The highest genotoxic response was observed for the August samples, whereas the highest oxidative stress response was recorded for the October samples, indicating that oxidative stress alone is not responsible for the genotoxicity. Previously, similar findings indicating an oxidative stress-independent genotoxicity pathway has been reported (Dumax-Vorzet et al., 2015). The decreasing proinflammatory responses elicited by this size range makes assessing the effects of inflammation on the genotoxic response difficult; in addition, harvesting the cells 24 h after the start of the exposure may be too short a time to observe secondary inflammation-induced genotoxicity.

In summary, the PM_{10-2.5} samples in the current study caused high levels of oxidative stress and genotoxicity in A549 cells. They also produced very high proinflammatory IL-8/CXCL8 levels for the smallest PM doses, which declined with increasing dosage. The oxidative stress likely influences the genotoxic response through oxidative DNA damage, whereas the declining inflammatory response is probably caused by composition-dependent inhibition of IL-8/CXCL8 production or secretion.

5. Conclusions

We observed substantial differences in the chemical composition and toxicological characteristics of size segregated urban air PM samples, collected in August and October 2013 from Nanjing, caused by distinctly varied emission sources, air mass trajectories, and atmospheric processes. Moreover, the PM composition and induced toxicological responses varied between the day and nighttime samples, indicating the influence of day-night variations of both atmospheric processes and emissions. The greatest toxicological responses were detected for the PM_{0.2} and PM_{10-2.5} size ranges for different endpoints, which suggests that both particle size and differing chemical composition affect which toxicological pathways are activated. The cell cycle disruption of A549 cells dominated the responses of PM collected in October, which has probably been caused by increased contributions of coal and biomass combustion emissions largely from the heavily industrialized Northern China, illustrated by the high levels of combustion-related metals and PAH species. Instead, the high cytotoxicity and inflammatory responses for the August PM samples were likely influenced by increased agricultural activity and soil preparation, long-range transported PM from the densely populated Yangtze River Delta region and Northern China, as well as by possible enrichment of certain harmful local or regional emissions.

Supplementary data to this article can be found online at <https://doi.org/10.1016/j.scitenv.2018.05.260>.

Acknowledgements

The authors wish to thank Hanne Vainikainen, Suvi Tossavainen and Henri Hakkarainen for their efforts and technical expertise in the present study.

Funding

This work was supported by the Academy of Finland (grants 278269, 278331, 287982, 294081, and 304459) and the University of Eastern Finland Doctoral School. The funding sources were not involved in the design, execution, or reporting of the current study.

References

- Akhtar, U.S., McWhinney, R.D., Rastogi, N., Abbott, J.P.D., Evans, G.J., Scott, J.A., 2010. Cytotoxic and proinflammatory effects of ambient and source-related particulate matter

- (PM) in relation to the production of reactive oxygen species (ROS) and cytokine adsorption by particles. *Inhal. Toxicol.* 22:37–47. <https://doi.org/10.3109/08958378.2010.518377>.
- Bai, H., Wu, M., Zhang, H., Tang, G., 2017. Chronic polycyclic aromatic hydrocarbon exposure causes DNA damage and genomic instability in lung epithelial cells. *Oncotarget* 8 (45):79034–79045. <https://doi.org/10.18632/oncotarget.20891>.
- Chen, N., Xu, L., 2017. Relationship between air quality and economic development in the provincial capital cities of China. *Environ. Sci. Pollut. Res.* 24 (3):2928–2935. <https://doi.org/10.1007/s11356-016-8065-3>.
- Chen, J., Li, C., Ristovski, Z., Milic, A., Gu, Y., Islam, M.S., Dumka, U.C., 2017a. A review of biomass burning: emissions and impacts on air quality, health and climate in China. *Sci. Total Environ.* 579:1000–1034. <https://doi.org/10.1016/j.scitotenv.2016.11.025>.
- Chen, P., Wang, T., Dong, M., Kasoar, M., Han, Y., Xie, M., Huang, T., 2017b. Characterization of major natural and anthropogenic source profiles for size-fractionated PM in Yangtze River delta. *Sci. Total Environ.* 598 (Supplement C):135–145. <https://doi.org/10.1016/j.scitotenv.2017.04.106>.
- Chen, P., Wang, T., Lu, X., Yu, Y., Kasoar, M., Xie, M., Zhuang, B., 2017c. Source apportionment of size-fractionated particles during the 2013 Asian Youth Games and the 2014 Youth Olympic Games in Nanjing, China. *Sci. Total Environ.* 579 (Supplement C):860–870. <https://doi.org/10.1016/j.scitotenv.2016.11.014>.
- Chow, J.C., Watson, J.G., Chen, L.-A., Arnott, W.P., Moosmüller, H., Fung, K., 2004. Equivalence of elemental carbon by thermal/optical reflectance and transmittance with different temperature protocols. *Environ. Sci. Technol.* 38 (16):4414–4422. <https://doi.org/10.1021/es034936u>.
- Cohen, A.J., Brauer, M., Burnett, R., Anderson, H.R., Frostad, J., Estep, K., Forouzanfar, M.H., 2017. Estimates and 25-year trends of the global burden of disease attributable to ambient air pollution: an analysis of data from the global burden of diseases study 2015. *Lancet* 389 (10082):1907–1918. [https://doi.org/10.1016/S0140-6736\(17\)30505-6](https://doi.org/10.1016/S0140-6736(17)30505-6).
- Dat, N., Chang, M.B., 2017. Review on characteristics of PAHs in atmosphere, anthropogenic sources and control technologies. *Sci. Total Environ.* 609 (Supplement C):682–693. <https://doi.org/10.1016/j.scitotenv.2017.07.204>.
- de Kok, T.M., Drieeck, H.A.L., Hogervorst, J.G.F., Briedé, J.J., 2006. Toxicological assessment of ambient and traffic-related particulate matter: a review of recent studies. *Mutat. Res. Rev. Mutat. Res.* 613 (2):103–122. <https://doi.org/10.1016/j.mrrev.2006.07.001>.
- Deng, X., Zhang, F., Rui, W., Long, F., Wang, L., Feng, Z., Ding, W., 2013. PM2.5-induced oxidative stress triggers autophagy in human lung epithelial A549 cells. *Toxicol. in Vitro* 27 (6):1762–1770. <https://doi.org/10.1016/j.tiv.2013.05.004>.
- Di Filippo, P., Riccardi, C., Pomata, D., Buiarelli, F., 2010. Concentrations of PAHs, and nitro- and methyl-derivatives associated with a size-segregated urban aerosol. *Atmos. Environ.* 44 (23):2742–2749. <https://doi.org/10.1016/j.atmosenv.2010.04.035>.
- Ding, A.J., Fu, C.B., Yang, X.Q., Sun, J.N., Zheng, L.F., Xie, Y.N., Kulmala, M., 2013. Ozone and fine particle in the western Yangtze River delta: an overview of 1 yr data at the SORPES station. *Atmos. Chem. Phys.* 13 (11):5813–5830. <https://doi.org/10.5194/acp-13-5813-2013>.
- Draxler, R.R., Hess, G.D., 1997. Description of the HYSPLIT_4 modeling system. NOAA Tech. Memo. ERL ARL-224NOAA Air Resources Laboratory, Silver Spring, MD 24 pp.
- Draxler, R.R., Hess, G.D., 1998. An overview of the HYSPLIT_4 modeling system of trajectories, dispersion, and deposition. *Aust. Meteor. Mag.* 47, 295–308.
- Draxler, R.R., 1999. HYSPLIT4 user's guide. NOAA Tech. Memo. ERL ARL-230NOAA Air Resources Laboratory, Silver Spring, MD.
- Duez, P., Dehon, G., Kumps, A., Dubois, J., 2003. Statistics of the comet assay: a key to discriminate between genotoxic effects. *Mutagenesis* 18 (2):159–166. <https://doi.org/10.1093/mutage/18.2.159>.
- Dumax-Vorzet, A.F., Tate, M., Walsmley, R., Elder, R.H., Povey, A.C., 2015. Cytotoxicity and genotoxicity of urban particulate matter in mammalian cells. *Mutagenesis* 30 (5):621–633. <https://doi.org/10.1093/mutage/geo205>.
- Fang, T., Guo, H., Zeng, L., Verma, V., Nenes, A., Weber, R.J., 2017. Highly acidic ambient particles, soluble metals, and oxidative potential: a link between sulfate and aerosol toxicity. *Environ. Sci. Technol.* 51 (5):2611–2620. <https://doi.org/10.1021/acs.est.6b01615>.
- Forouzanfar, M.H., Alexander, L., Anderson, H.R., Bachman, V.F., Biryukov, S., Brauer, M., Murray, C.J., 2015. Global, regional, and national comparative risk assessment of 79 behavioural, environmental and occupational, and metabolic risks or clusters of risks in 188 countries, 1990–2013: a systematic analysis for the global burden of disease study 2013. *Lancet* 386 (10010):2287–2323. [https://doi.org/10.1016/S0140-6736\(15\)00128-2](https://doi.org/10.1016/S0140-6736(15)00128-2).
- Fu, F., Tian, B., Lin, G., Chen, Y., Zhang, J., 2010. Chemical characterization and source identification of polycyclic aromatic hydrocarbons in aerosols originating from different sources. *J. Air Waste Manage. Assoc.* 60 (11):1309–1314. <https://doi.org/10.3155/1047-3289.60.11.1309>.
- Fu, P.P., Xia, Q., Sun, X., Yu, H., 2012. Phototoxicity and environmental transformation of polycyclic aromatic hydrocarbons (PAHs)—light-induced reactive oxygen species, lipid peroxidation, and DNA damage. *J. Environ. Sci. Health C* 30 (1):1–41. <https://doi.org/10.1080/10590501.2012.653887>.
- Genies, C., Jullien, A., Lefebvre, E., Revol, M., Maitre, A., Douki, T., 2016. Inhibition of the formation of benzo[a]pyrene adducts to DNA in A549 lung cells exposed to mixtures of polycyclic aromatic hydrocarbons. *Toxicol. in Vitro* 35 (Supplement C):1–10. <https://doi.org/10.1016/j.tiv.2016.05.006>.
- Ghio, A.J., Kummarapurugu, S.T., Tong, H., Soukup, J.M., Dailey, L.A., Boykin, E., Reynolds, R.L., 2014. Biological effects of desert dust in respiratory epithelial cells and a murine model. *Inhal. Toxicol.* 26 (5):299–309. <https://doi.org/10.3109/08958378.2014.888109>.
- Grahame, T.J., Schlesinger, R.B., 2005. Evaluating the health risk from secondary sulfates in Eastern North American regional ambient air particulate matter. *Inhal. Toxicol.* 17 (1):15–27. <https://doi.org/10.1080/08958370590885672>.
- Guo, L., Zhang, Y., Lin, H., Zeng, W., Liu, T., Xiao, J., Ma, W., 2016. The washout effects of rainfall on atmospheric particulate pollution in two Chinese cities. *Environ. Pollut.* 215:195–202. <https://doi.org/10.1016/j.envpol.2016.05.003>.
- Happo, M.S., Salonen, R.O., Hälinen, A.I., Jalava, P.I., Pennanen, A.S., Kosma, V.M., Hirvonen, M.-R., 2007. Dose and time dependency of inflammatory responses in the mouse lung to urban air coarse, fine, and ultrafine particles from six European cities. *Inhal. Toxicol.* 19:227–246. <https://doi.org/10.1080/08958370601067897>.
- Happo, M.S., Hirvonen, M.-R., Hälinen, A.I., Jalava, P.I., Pennanen, A.S., Sillanpää, M., Salonen, R.O., 2008. Chemical compositions responsible for inflammation and tissue damage in the mouse lung by coarse and fine particulate samples from contrasting air pollution in Europe. *Inhal. Toxicol.* 20 (14):1215–1231. <https://doi.org/10.1080/08958370802147282>.
- Happo, M.S., Hirvonen, M.-R., Hälinen, A.I., Jalava, P.I., Pennanen, A.S., Sillanpää, M., Salonen, R.O., 2010a. Seasonal variation in chemical composition of size-segregated urban air particles and the inflammatory activity in the mouse lung. *Inhal. Toxicol.* 22 (1):17–32. <https://doi.org/10.3109/08958370902862426>.
- Happo, M.S., Salonen, R.O., Hälinen, A.I., Jalava, P.I., Pennanen, A.S., Dormans, J.A.M.A., Hirvonen, M.-R., 2010b. Inflammation and tissue damage in mouse lung by single and repeated dosing of urban air coarse and fine particles collected from six European cities. *Inhal. Toxicol.* 22 (5):402–416. <https://doi.org/10.3109/08958370903527908>.
- Hetland, R.B., Myhre, O., Låg, M., Hongve, D., Schwarze, P.E., Refsnes, M., 2001. Importance of soluble metals and reactive oxygen species for cytokine release induced by mineral particles. *Toxicology* 165 (2):133–144. [https://doi.org/10.1016/S0300-483X\(01\)00418-8](https://doi.org/10.1016/S0300-483X(01)00418-8).
- Hleis, D., Fernández-Olmo, I., Ledoux, F., Kfouri, A., Courcot, L., Desmonts, T., Courcot, D., 2013. Chemical profile identification of fugitive and confined particle emissions from an integrated iron and steelmaking plant. *J. Hazard. Mater.* 250–251 (Supplement C):246–255. <https://doi.org/10.1016/j.jhazmat.2013.01.080>.
- Hu, X., Ding, Z., Zhang, Y., Sun, Y., Wu, J., Chen, Y., Lian, H., 2013. Size distribution and source apportionment of airborne metallic elements in Nanjing, China. *Aerosol Air Qual. Res.* 13 (6):1796–1806. <https://doi.org/10.4209/aaqr.2012.11.0332>.
- Huang, Q., Zhang, J., Peng, S., Tian, M., Chen, J., Shen, H., 2014. Effects of water soluble PM2.5 extracts exposure on human lung epithelial cells (A549): a proteomic study. *J. Appl. Toxicol.* 34 (6):675–687. <https://doi.org/10.1002/jat.2910>.
- Itahashi, S., Hayami, H., Yumimoto, K., Uno, I., 2016. Chinese province-scale source apportionments for sulfate aerosols in 2005 evaluated by the tagged tracer method. *Environ. Pollut.* 220:1366–1375. <https://doi.org/10.1016/j.envpol.2016.10.098>.
- Jalava, P.I., Salonen, R.O., Hälinen, A.I., Penttilä, P., Pennanen, A.S., Sillanpää, M., Hirvonen, M.-R., 2006. In vitro inflammatory and cytotoxic effects of size-segregated particulate samples collected during long-range transport of wildfire smoke to Helsinki. *Toxicol. Appl. Pharmacol.* 215 (3):341–353. <https://doi.org/10.1016/j.taap.2006.03.007>.
- Jalava, P.I., Salonen, R.O., Pennanen, A.S., Sillanpää, M., Hälinen, A.I., Happo, M.S., Hirvonen, M.-R., 2007. Heterogeneities in inflammatory and cytotoxic responses of RAW 264.7 macrophage cell line to urban air coarse, fine, and ultrafine particles from six European sampling campaigns. *Inhal. Toxicol.* 19 (3):213–225. <https://doi.org/10.1080/0895837061067863>.
- Jalava, P.I., Hirvonen, M.-R., Sillanpää, M., Pennanen, A.S., Happo, M.S., Hirvonen, M.-R., Salonen, R.O., 2009. Associations of urban air particulate composition with inflammatory and cytotoxic responses in RAW 264.7 cell line. *Inhal. Toxicol.* 21 (12):994–1006. <https://doi.org/10.1080/08958370802695710>.
- Jalava, P.I., Wang, Q., Kuuspaloo, K., Ruusunen, J., Hao, L., Fang, D., Hirvonen, M.-R., 2015. Day and night variation in chemical composition and toxicological responses of size segregated urban air PM samples in a high air pollution situation. *Atmos. Environ.* 120:427–437. <https://doi.org/10.1016/j.atmosenv.2015.08.089>.
- Jalava, P.I., Happo, M.S., Huttunen, K., Sillanpää, M., Hirvonen, M.-R., 2016. Chemical and microbial components of urban air PM cause seasonal variation of toxicological activity. *Environ. Toxicol. Pharmacol.* 40 (2):375–387. <https://doi.org/10.1016/j.etap.2015.06.023>.
- Janssen, N.A.H., Yang, A., Strak, M., Steenhof, M., Hellack, B., Gerlofs-Nijland, M.E., Cassee, F., 2014. Oxidative potential of particulate matter collected at sites with different source characteristics. *Sci. Total Environ.* 472 (Supplement C):572–581. <https://doi.org/10.1016/j.scitotenv.2013.11.099>.
- Kang, Y., Liu, M., Song, Y., Huang, X., Yao, H., Cai, X., Zhu, T., 2016. High-resolution ammonia emissions inventories in China from 1980 to 2012. *Atmos. Chem. Phys.* 16 (4):2043–2058. <https://doi.org/10.5194/acp-16-2043-2016>.
- Kasurinen, S., Jalava, P.I., Happo, M.S., Sippula, O., Uski, O., Koponen, H., Hirvonen, M.-R., 2017. Particulate emissions from the combustion of birch, beech, and spruce logs cause different cytotoxic responses in A549 cells. *Environ. Toxicol.* 32 (5):1487–1499. <https://doi.org/10.1002/tox.22369>.
- Kim, K., Jahan, S.A., Kabir, E., Brown, R.J.C., 2013. A review of airborne polycyclic aromatic hydrocarbons (PAHs) and their human health effects. *Environ. Int.* 60 (Supplement C):71–80. <https://doi.org/10.1016/j.envint.2013.07.019>.
- Knaapen, A.M., Shi, T., Borm, P.J.A., Schins, R.P.F., 2002. Soluble metals as well as the insoluble particle fraction are involved in cellular DNA damage induced by particulate matter. *Mol. Cell. Biochem.* 234 (1):317–326. <https://doi.org/10.1023/A:1015970023889>.
- Koike, E., Yanagisawa, R., Takano, H., 2014. Toxicological effects of polycyclic aromatic hydrocarbons and their derivatives on respiratory cells. *Atmos. Environ.* 97 (Supplement C):529–536. <https://doi.org/10.1016/j.atmosenv.2014.04.003>.
- Könözöl, M., Goldenberg, E., Ebeling, S., Schäfer, B., García-Käufer, M., Gminski, R., Mersch-Sundermann, V., 2012. Cellular uptake and toxic effects of fine and ultrafine metal-sulfate particles in human A549 lung epithelial cells. *Chem. Res. Toxicol.* 25 (12):2687–2703. <https://doi.org/10.1021/tx300333z>.
- Könözöl, M., Weiss, A., Stangenber, E., Gminski, R., García-Käufer, M., Gieré, R., Mersch-Sundermann, V., 2013. Cell-cycle changes and oxidative stress response to magnetite in A549 human lung cells. *Chem. Res. Toxicol.* 26 (5):693–702. <https://doi.org/10.1021/tx300333q>.
- Künzli, N., Mudway, I.S., Götschi, T., Shi, T., Kelly, F.J., Cook, S., Borm, P.J.A., 2006. Comparison of oxidative properties, light absorbance, and total and elemental mass

- concentration of ambient PM2.5 collected at 20 European sites. *Environ. Health Perspect.* 114 (5):684–690. <https://doi.org/10.1289/ehp.8584>.
- Landkocz, Y., Ledoux, F., André, V., Cazier, F., Genevray, P., Dewaele, D., Billet, S., 2017. Fine and ultrafine atmospheric particulate matter at a multi-influenced urban site: physicochemical characterization, mutagenicity and cytotoxicity. *Environ. Pollut.* 221 (Supplement C):130–140. <https://doi.org/10.1016/j.envpol.2016.11.054>.
- Li, H., Han, Z., Cheng, T., Du, H., Kong, L., Chen, J., Wang, W., 2010. Agricultural fire impacts on the air quality of Shanghai during summer harvesttime. *Aerosol Air Qual. Res.* 10 (2):95–101. <https://doi.org/10.4209/aaqr.2009.08.0049>.
- Li, K., Chen, L., Ying, F., White, S.J., Jang, C., Wu, X., Cen, K., 2017. Meteorological and chemical impacts on ozone formation: a case study in Hangzhou, China. *Atmos. Res.* 196 (Supplement C):40–52. <https://doi.org/10.1016/j.atmosres.2017.06.003>.
- Líbalová, H., Krčková, Š., Uhliřová, K., Milcová, A., Schmuczerová, J., Čigánek, M., Topinka, J., 2014. Genotoxicity but not the AhR-mediated activity of PAHs is inhibited by other components of complex mixtures of ambient air pollutants. *Toxicol. Lett.* 225 (3): 350–357. <https://doi.org/10.1016/j.toxlet.2014.01.028>.
- Lim, S.S., Vos, T., Flaxman, A.D., Danaei, G., Shibuya, K., Adair-Rohani, H., Ezzati, M., 2012. A comparative risk assessment of burden of disease and injury attributable to 67 risk factors and risk factor clusters in 21 regions, 1990–2010: a systematic analysis for the global burden of disease study 2010. *Lancet* 380 (9859):2224–2260. [https://doi.org/10.1016/S0140-6736\(12\)61766-8](https://doi.org/10.1016/S0140-6736(12)61766-8).
- Liu, Q., Baumgartner, J., Zhang, Y., Liu, Y., Sun, Y., Zhang, M., 2014. Oxidative potential and inflammatory impacts of source apportioned ambient air pollution in Beijing. *Environ. Sci. Technol.* 48 (21):12920–12929. <https://doi.org/10.1021/es5029876>.
- Machemer, S.D., 2004. Characterization of airborne and bulk particulate from iron and steel manufacturing facilities. *Environ. Sci. Technol.* 38 (2):381–389. <https://doi.org/10.1021/es020897v>.
- Maher, B.A., Ahmed, I.A.M., Karloukovski, V., MacLaren, D.A., Foulds, P.G., Allsop, D., Calderon-Garcidueñas, L., 2016. Magnetite pollution nanoparticles in the human brain. *Proc. Natl. Acad. Sci.* 113 (39):10797–10801. <https://doi.org/10.1073/pnas.1605941113>.
- Mattsson, Å., Jernström, B., Cotgreave, I.A., Bajak, E., 2009. H2AX phosphorylation in A549 cells induced by the bulky and stable DNA adducts of benzo[a]pyrene and dibenzo[a, l]pyrene diol epoxides. *Chem. Biol. Interact.* 177 (1):40–47. <https://doi.org/10.1016/j.cbi.2008.09.015>.
- Mazidi, M., Speakman, J.R., 2017. Ambient particulate air pollution (PM2.5) is associated with the ratio of type 2 diabetes to obesity. *Sci. Rep.* 7 (1):9144. <https://doi.org/10.1038/s41598-017-08287-1>.
- Meng, Q., Fan, S., He, J., Zhang, J., Sun, Y., Zhang, Y., Zu, F., 2015. Particle size distribution and characteristics of polycyclic aromatic hydrocarbons during a heavy haze episode in Nanjing, China. *Particuology* 18 (Supplement C):127–134. <https://doi.org/10.1016/j.partic.2014.03.010>.
- Michael, S., Montag, M., Dott, W., 2013. Pro-inflammatory effects and oxidative stress in lung macrophages and epithelial cells induced by ambient particulate matter. *Environ. Pollut.* 183 (Supplement C):19–29. <https://doi.org/10.1016/j.envpol.2013.01.026>.
- Motoyama, Y., Bekki, K., Chung, S.W., Tang, N., Kameda, T., Toriba, A., Hayakawa, K., 2009. Oxidative stress more strongly induced by *ortho*- than *para*-quinoid polycyclic aromatic hydrocarbons in A549 cells. *J. Health Sci.* 55 (5):845–850. <https://doi.org/10.1248/jhs.55.845>.
- Orasche, J., Seidel, T., Hartmann, H., Schnelle-Kreis, J., Chow, J.C., Ruppert, H., Zimmermann, R., 2012. Comparison of emissions from wood combustion. Part 1: emission factors and characteristics from different small-scale residential heating appliances considering particulate matter and polycyclic aromatic hydrocarbon (PAH)-related toxicological potential of particle-bound organic species. *Energy Fuel* 26 (11): 6695–6704. <https://doi.org/10.1021/ef301295k>.
- Orasche, J., Schnelle-Kreis, J., Schön, C., Hartmann, H., Ruppert, H., Arteaga-Salas, J., Zimmermann, R., 2013. Comparison of emissions from wood combustion. Part 2: impact of combustion conditions on emission factors and characteristics of particle-bound organic species and polycyclic aromatic hydrocarbon (PAH)-related toxicological potential. *Energy Fuel* 27 (3):1482–1491. <https://doi.org/10.1021/ef301506h>.
- Oros, D.R., Simoneit, B.R.T., 2000. Identification and emission rates of molecular tracers in coal smoke particulate matter. *Fuel* 79 (5):515–536. [https://doi.org/10.1016/S0016-2361\(99\)00153-2](https://doi.org/10.1016/S0016-2361(99)00153-2).
- Pearson, J.F., Bachireddy, C., Shyamprasad, S., Goldfine, A.B., Brownstein, J.S., 2010. Association between fine particulate matter and diabetes prevalence in the U.S. *Diabetes Care* 33 (10):2196–2201. <https://doi.org/10.2337/dc10-0698>.
- Penning, T.M., Burczynski, M.E., Hung, C., McColl, K.D., Palackal, N.T., Tsuruda, L.S., 1999. Dihydrodiol dehydrogenases and polycyclic aromatic hydrocarbon activation: generation of reactive and redox active o-quinones. *Chem. Res. Toxicol.* 12 (1):1–18. <https://doi.org/10.1021/tx980143n>.
- Perrone, M.G., Gualtieri, M., Ferrero, L., Porto, C.L., Udisti, R., Bolzacchini, E., Camatini, M., 2010. Seasonal variations in chemical composition and in vitro biological effects of fine PM from Milan. *Chemosphere* 78 (11):1368–1377. <https://doi.org/10.1016/j.chemosphere.2009.12.071>.
- Perrone, M.G., Gualtieri, M., Consonni, V., Ferrero, L., Sangiorgi, G., Longhin, E., Camatini, M., 2013. Particle size, chemical composition, seasons of the year and urban, rural or remote site origins as determinants of biological effects of particulate matter on pulmonary cells. *Environ. Pollut.* 176:215–227. <https://doi.org/10.1016/j.envpol.2013.01.012>.
- Qi, L., Zhang, Y., Ma, Y., Chen, M., Ge, X., Ma, Y., Li, S., 2016. Source identification of trace elements in the atmosphere during the second Asian Youth Games in Nanjing, China: influence of control measures on air quality. *Atmos. Pollut. Res.* 7 (3): 547–556. <https://doi.org/10.1016/j.apr.2016.01.003>.
- Ravindra, K., Sokhi, R., Van Grieken, R., 2008. Atmospheric polycyclic aromatic hydrocarbons: source attribution, emission factors and regulation. *Atmos. Environ.* 42 (13): 2895–2921. <https://doi.org/10.1016/j.atmosenv.2007.12.010>.
- Reiss, R., Anderson, E.L., Cross, C.E., Hidy, G., Hoel, D., McClellan, R., Moolgavkar, S., 2007. Evidence of health impacts of sulfate-and nitrate-containing particles in ambient air. *Inhal. Toxicol.* 19 (5):419–449. <https://doi.org/10.1080/08958370601174941>.
- Ringuet, J., Albinet, A., Leoz-Garzandia, E., Budzinski, H., Villenave, E., 2012. Reactivity of polycyclic aromatic compounds (PAHs, NPAHs and OPAs) adsorbed on natural aerosol particles exposed to atmospheric oxidants. *Atmos. Environ.* 61:15–22. <https://doi.org/10.1016/j.atmosenv.2012.07.025>.
- Roos, W.P., Thomas, A.D., Kaina, B., 2016. DNA damage and the balance between survival and death in cancer biology. *Nat. Rev. Cancer* 16 (1):20–33. <https://doi.org/10.1038/nrc.2015.2>.
- Ruan, R., Tan, H., Wang, X., Li, Y., Li, S., Hu, Z., Yang, T., 2018. Characteristics of fine particulate matter formation during combustion of lignite riched in AAEM (alkali and alkaline earth metals) and sulfur. *Fuel* 211:206–213. <https://doi.org/10.1016/j.fuel.2017.08.114>.
- Sawyer, K., Mundandharra, S., Ghio, A.J., Madden, M.C., 2009. The effects of ambient particulate matter on human alveolar macrophage oxidative and inflammatory responses. *J. Toxic. Environ. Health A* 73 (1):41–57. <https://doi.org/10.1080/15287390903248901>.
- Schlesinger, R.B., 2007. The health impact of common inorganic components of fine particulate matter (PM2.5) in ambient air: a critical review. *Inhal. Toxicol.* 19 (10): 811–832. <https://doi.org/10.1080/08958370701402382>.
- Schlesinger, R.B., Cassee, F., 2003. Atmospheric secondary inorganic particulate matter: the toxicological perspective as a basis for health effects risk assessment. *Inhal. Toxicol.* 15 (3):197. <https://doi.org/10.1080/08958370304503>.
- Schwarze, P.E., Øvrevik, J., Låg, M., Refsnes, M., Nafstad, P., Hetland, R.B., Dybing, E., 2006. Particulate matter properties and health effects: consistency of epidemiological and toxicological studies. *Hum. Exp. Toxicol.* 25 (10):559–579. <https://doi.org/10.1177/096032706072520>.
- Seinfeld, J.H., Pandis, S.N., 2006. *Atmospheric Chemistry and Physics*. Wiley, Hoboken, NJ.
- Shu, W., Zhao, Y., Ni, H., Zeng, H., 2018. Size-dependent emission characteristics of airborne parent and halogenated PAHs from municipal solid waste incinerators in Shenzhen, China. *Chemosphere* 192 (Supplement C):250–257. <https://doi.org/10.1016/j.chemosphere.2017.10.155>.
- Sillanpää, M., Hillamo, R., Mäkelä, T., Pennanen, A.S., Salonen, R.O., 2003. Field and laboratory tests of a high volume cascade impactor. *J. Aerosol Sci.* 34 (4):485–500. [https://doi.org/10.1016/S0021-8502\(02\)00214-8](https://doi.org/10.1016/S0021-8502(02)00214-8).
- Silliman, S., 1995. The use of NO_x, H₂O₂, and HNO₃ as indicators for ozone-NO_x-hydrocarbon sensitivity in urban locations. *J. Geophys. Res.* 100 (D7: 14,188). <https://doi.org/10.1029/94JD02953>.
- Silva, R.A., Adelman, Z., Fry, M.M., West, J.J., 2016. The impact of individual anthropogenic emissions sectors on the global burden of human mortality due to ambient air pollution. *Environ. Health Perspect.* 124 (11):1776–1784. <https://doi.org/10.1289/EHP177>.
- Simoneit, B.R.T., Rogge, W.F., Lang, Q., Jaffé, R., 2000. Molecular characterization of smoke from campfire burning of pine wood (*Pinus elliottii*). *Chemosphere Global Change Sci.* 2 (1):107–122. [https://doi.org/10.1016/S1465-9792\(99\)00048-3](https://doi.org/10.1016/S1465-9792(99)00048-3).
- Sippula, O., Rintala, H., Happo, M., Jalava, P., Kuuspalo, K., Virén, A., Hirvonen, M.-R., 2013. Characterization of chemical and microbial species from size-segregated indoor and outdoor particulate samples. *Aerosol Air Qual. Res.* 13:1212–1230. <https://doi.org/10.4209/aaqr.2012.11.0300>.
- Sklorz, M., Briedé, J., Schnelle-Kreis, J., Liu, Y., Cyrys, J., de Kok, T.M., Zimmermann, R., 2007. Concentration of oxygenated polycyclic aromatic hydrocarbons and oxygen free radical formation from urban particulate matter. *J. Toxic. Environ. Health A* 70 (21):1866–1869. <https://doi.org/10.1080/15287390701457654>.
- Soberanes, S., Urich, D., Baker, C.M., Burgess, Z., Chiarella, S.E., Bell, E.L., Budinger, G.R.S., 2009. Mitochondrial complex III-generated oxidants activate ASK1 and JNK to induce alveolar epithelial cell death following exposure to particulate matter air pollution. *J. Biol. Chem.* 284 (4), 2176–2186.
- Soukup, J.M., Becker, S., 2001. Human alveolar macrophage responses to air pollution particulates are associated with insoluble components of coarse material, including particulate endotoxin. *Toxicol. Appl. Pharmacol.* 171 (1):20–26. <https://doi.org/10.1006/taap.2000.9096>.
- Squizzato, S., Masiol, M., Brunelli, A., Pistollato, S., Tarabotti, E., Rampazzo, G., Pavoni, B., 2013. Factors determining the formation of secondary inorganic aerosol: a case study in the Po valley (Italy). *Atmos. Chem. Phys.* 13 (4):1927–1939. <https://doi.org/10.5194/acp-13-1927-2013>.
- Steenhof, M., Gossens, I., Strak, M., Godri, K.J., Hoek, G., Cassee, F.R., Pieters, R.H.H., 2011. In vitro toxicity of particulate matter (PM) collected at different sites in the Netherlands is associated with PM composition, size fraction and oxidative potential - the RAPTES project. *Part. Fibre Toxicol.* 8 (1):26. <https://doi.org/10.1186/1743-8977-8-26>.
- Stein, A.F., Draxler, R.R., Rolph, G.D., Stunder, B.J.B., Cohen, M.D., Ngan, F., 2015. NOAA's HYSPLIT atmospheric transport and dispersion modeling system. *Bull. Amer. Meteor. Soc.* 96:2059–2077. <https://doi.org/10.1175/BAMS-D-14-00110.1>.
- Stockwell, W.R., Kuhns, H., Etyemezian, V., Green, M.C., Chow, J.C., Watson, J.G., 2003. The treasure valley secondary aerosol study II: modeling of the formation of inorganic secondary aerosols and precursors for southwestern Idaho. *Atmos. Environ.* 37 (4): 525–534. [https://doi.org/10.1016/S1352-2310\(02\)00895-6](https://doi.org/10.1016/S1352-2310(02)00895-6).
- Sunjog, K., Kolarević, S., Héberger, K., Gaćić, Z., Knežević-Vukčević, J., Vuković-Gaćić, B., Lenhardt, M., 2013. Comparison of comet assay parameters for estimation of genotoxicity by sum of ranking differences. *Anal. Bioanal. Chem.* 405 (14): 4879–4885. <https://doi.org/10.1007/s00216-013-6909-y>.
- Tang, G., Zhang, J., Zhu, X., Song, T., Mükel, C., Hu, B., Wang, Y., 2016. Mixing layer height and its implications for air pollution over Beijing, China. *Atmos. Environ. Chem.* 16 (4): 2459–2475. <https://doi.org/10.5194/acp-16-2459-2016>.
- Tapanainen, M., Jalava, P.I., Mäki-Paakkonen, J., Hakulinen, P., Lamberg, H., Ruusunen, J., Hirvonen, M.-R., 2012. Efficiency of log wood combustion affects the toxicological

- and chemical properties of emission particles. *Inhal. Toxicol.* 24 (6):343–355. <https://doi.org/10.3109/08958378.2012.671858>.
- Teixeira, E.C., Agudelo-Castañeda, D.M., Fachel, J.M.G., Leal, K.A., Garcia, K.d.O., Wiegand, F., 2012. Source identification and seasonal variation of polycyclic aromatic hydrocarbons associated with atmospheric fine and coarse particles in the metropolitan area of Porto Alegre, RS, Brazil. *Atmos. Res.* 118 (Supplement C):390–403. <https://doi.org/10.1016/j.atmosres.2012.07.004>.
- Valavanidis, A., Vlachogianni, T., Fiotakis, K., Loridas, S., 2013. Pulmonary oxidative stress, inflammation and cancer: respirable particulate matter, fibrous dusts and ozone as major causes of lung carcinogenesis through reactive oxygen species mechanisms. *Int. J. Environ. Res. Public Health* 10 (9):3886–3907. <https://doi.org/10.3390/ijerph10093886>.
- Verma, V., Ning, Z., Cho, A.K., Schauer, J.J., Shafer, M.M., Sioutas, C., 2009. Redox activity of urban quasi-ultrafine particles from primary and secondary sources. *Atmos. Environ.* 43 (40):6360–6368. <https://doi.org/10.1016/j.atmosenv.2009.09.019>.
- Walgraeve, C., Demeestere, K., Dewulf, J., Zimmermann, R., Van Langenhove, H., 2010. Oxygenated polycyclic aromatic hydrocarbons in atmospheric particulate matter: molecular characterization and occurrence. *Atmos. Environ.* 44 (15):1831–1846. <https://doi.org/10.1016/j.atmosenv.2009.12.004>.
- Wang, W., Jariyasopit, N., Schrlau, J., Jia, Y., Tao, S., Yu, T., Simonich, S.L.M., 2011. Concentration and photochemistry of PAHs, NPAHs, and OPAHs and toxicity of PM2.5 during the Beijing Olympic games. *Environ. Sci. Technol.* 45 (16):6887–6895. <https://doi.org/10.1021/es201443z>.
- Wang, S., Nan, J., Shi, C., Fu, Q., Gao, S., Wang, D., Zhou, B., 2015. Atmospheric ammonia and its impacts on regional air quality over the megacity of Shanghai, China. *Sci. Rep.* 5:15842. <https://doi.org/10.1038/srep15842>.
- Wang, H., An, J., Cheng, M., Shen, L., Zhu, B., Li, Y., Xia, L., 2016. One year online measurements of water-soluble ions at the industrially polluted town of Nanjing, China: sources, seasonal and diurnal variations. *Chemosphere* 148 (Supplement C): 526–536. <https://doi.org/10.1016/j.chemosphere.2016.01.066>.
- Wei, S., Huang, B., Liu, M., Bi, X., Ren, Z., Sheng, G., Fu, J., 2012. Characterization of PM2.5-bound nitrated and oxygenated PAHs in two industrial sites of South China. *Atmos. Res.* 109–110 (Supplement C):76–83. <https://doi.org/10.1016/j.atmosres.2012.01.009>.
- World Health Organization, International Programme on Chemical Safety, 1998. *Selected Non-Heterocyclic Polycyclic Aromatic Hydrocarbons*. World Health Organization, Geneva.
- Yang, W., Zhu, Y., Cheng, W., Sang, H., Yang, H., Chen, H., 2017. Characteristics of particulate matter emitted from agricultural biomass combustion. *Energy Fuel* 31 (7): 7493–7501. <https://doi.org/10.1021/acs.energyfuels.7b00229>.
- Ying, Q., Wu, L., Zhang, H., 2014. Local and inter-regional contributions to PM2.5 nitrate and sulfate in China. *Atmos. Environ.* 94:582–592. <https://doi.org/10.1016/j.atmosenv.2014.05.078>.
- Yuan, F., Gao, J., Wang, L., Cai, Y., 2017. Co-location of manufacturing and producer services in Nanjing, China. *Cities* 63 (Supplement C):81–91. <https://doi.org/10.1016/j.cities.2016.12.021>.
- Yunker, M.B., Macdonald, R.W., Vingarzan, R., Mitchell, R.H., Goyette, D., Sylvestre, S., 2002. PAHs in the Fraser river basin: a critical appraisal of PAH ratios as indicators of PAH source and composition. *Org. Geochem.* 33 (4):489–515. [https://doi.org/10.1016/S0146-6380\(02\)00002-5](https://doi.org/10.1016/S0146-6380(02)00002-5).
- Zhang, X., McMurry, P.H., 1991. Theoretical analysis of evaporative losses of adsorbed or absorbed species during atmospheric aerosol sampling. *Environ. Sci. Technol.* 25 (3):456–459. <https://doi.org/10.1021/es00015a012>.
- Zhang, Y., Schauer, J.J., Zhang, Y., Zeng, L., Wei, Y., Liu, Y., Shao, M., 2008. Characteristics of particulate carbon emissions from real-world Chinese coal combustion. *Environ. Sci. Technol.* 42 (14):5068–5073. <https://doi.org/10.1021/es7022576>.
- Zhang, J., Yang, L., Mellouki, A., Chen, J., Chen, X., Gao, Y., Wang, W., 2017. Atmospheric PAHs, NPAHs, and OPAHs at an urban, mountainous, and marine sites in Northern China: molecular composition, sources, and ageing. *Atmos. Environ.* <https://doi.org/10.1016/j.atmosenv.2017.11.002>.
- Zhao, J., Yuan, Y., Ren, Y., Wang, H., 2015. Environmental assessment of crop residue processing methods in rural areas of Northeast China. *Renew. Energy* 84:22–29. <https://doi.org/10.1016/j.renene.2015.06.063>.
- Zhu, B., Su, J., Han, Z., Cong, Y., Wang, T., Cai, Y., 2010. Analysis of a serious air pollution event resulting from crop residue burning over Nanjing and surrounding regions. *Proc. SPIE Int. Soc. Opt. Eng.* 7809. <https://doi.org/10.1117/12.860353>.